Modelling Vertical Plate Radiators for Electric Transformers
Efacec

José Paulo Barbosa Baltazar

Dissertação do MIEM

Orientador na Efacec: Eng.º Hugo Campelo

Orientador na FEUP: Prof. Clito Afonso

Faculdade de Engenharia da Universidade do Porto

Mestrado Integrado em Engenharia Mecânica

Junho de 2014

Acknowledgments

I would like to acknowledge my supervisors on this work, Prof. Clito Afonso at the University and Eng.º Hugo Campelo at the company Efacec.

I would also like to thank my family, my friends and my girlfriend for all the support, encouragement and patience given during the entire course of Mechanical Engineering.

Abstract

In the electric conversion process of a transformer, some power is lost and converted into heat. These heat losses lead to temperature rises that have to be controlled with cooling solutions, since working with high temperatures lead to the deterioration of components and reduces the lifespan of the transformer. The coils and core of a transformer are usually immersed in an oil filled tank. For large transformers the oil is heated in this tank and then cooled in external heat exchangers. The typical heat exchangers used consists in thin vertical plate radiators, in which the oil transfers heat to the surrounding air.

The objective of this work was to create and evaluate calculation methodologies to predict the cooling capacity of vertical plate radiators. The developed methodologies use heat transfer correlations for oil and air in both natural and forced convection. For air natural convection, preliminary experiments were performed and results were compared with the calculation methodology using correlations from literature. The correlations were also applied to other two case studies and proved to have low accuracy on predicting the radiators cooling capacity. For air forced convection, CFD simulations were performed and results were compared to the calculation methodology. This comparison showed that the air flow between radiator's plates is not fully developed and that literature correlations do not take into account that phenomenon, causing an underestimation of the cooling capacity by the calculation methodology. New heat transfer correlations were developed for air forced convection using the CFD simulation data, in order to improve the calculation methodology. These new correlations presented great accuracy when applied to the radiators of a real transformer (cooling capacity deviations of 3.9% relatively to results from tests performed by Efacec company). The radiation heat transfer mode was included in the calculation methodologies and results showed that this is an important mechanism in radiators, especially when air convection is natural.

Nomenclature

c_p – specific heat at constant pressure [J/(kg.K)]

D_h – Hydraulic diameter [m]

F – View factor [-]

h – Convective heat transfer coefficient [W/(m^2.K)]

k – Thermal conductivity [W/(m.K)]

L - Plate length [m]

$\dot{m}$ – Mass flow rate [kg/s]

N – Number of plates per radiator [-]

Nu – Nusselt number [-]

P – Heat dissipation or cooling capacity [W]

Pr – Prandtl number [-]

Q – Volumetric flow rate [m^3/s]

R – Thermal resistance [K/W]

Ra – Rayleigh number [-]

Re – Reynolds number [-]

S - Distance between plates [m]

T – Temperature [ºC]

v – Velocity [m/s]

W - Plate width [m]

x_{fd} - Hydrodynamic entry length [m]

β – Coefficient of volumetric thermal expansion [K^{-1}]

ε – Emissivity [-]

μ – Dynamic viscosity [Pa.s]

ν – Kinematic viscosity [m^2/s]

ρ – Density [kg/m^3]

σ – Stefan–Boltzmann constant [W.m^{-2}.K^{-4}]

Subscripts:

ave – Average

channel – Of one oil channel

conv - Convection

end – On the radiator outer surfaces

ext – External

fan – Quantity per fan

fd – Fully developed

gap – On the radiator inner surfaces

plate – Quantity per plate

in - Inlet

int – Internal

out – Outlet

rad - Radiation

radiator – Quantity per radiator

transformer – Total quantity for the transformer

wall – On the wall

Table of Contents

1. Introduction

The first section of this chapter presents Efacec, the company where the work was developed. The second section introduces transformers and contextualizes the heat generation in this equipment. Then, after explaining the importance of cooling transformers efficiently, the project was described along with its objectives. Finally, in the last section is presented the organization of this work.

1.1. Presentation of Efacec

Efacec is a Portuguese company with business activity in the electric field, being present in more than 65 countries in the five continents. This company provides systems and solutions for the areas of energy, mobility and environment [1].

Design and manufacture of transformers is developed by Efacec, including power and distribution Transformers (Figure 1). Distribution includes dry type and oil immersed transformers, from 50 to 20000 kVA. Regarding power transformers, Efacec produces Shell and Core types with rated powers up to 1500 and 350 MVA, respectively. These two types differ in constructive aspects such as the coils' shape, the winding type and the magnetic core arrangement (vertical or horizontal).

Figure 1 – Examples of distribution (left) and power (right) transformers [1].

Efacec's Research and Development Department analyses, among other subjects, the electrical, magnetic and cooling behavior of transformers equipment in order to improve their efficiency and build new solutions.

1.2. Transformers and Heat Generation

The function of transformers is to change voltage levels between two circuits, being consequently modified the current values. Transformers have efficiency greater than 99% and consequently the input and output powers are nearly the same, being the lost power converted to heat. Since power transformers operate with great power levels, the heat losses will lead to temperature rise that have to be controlled by cooling [2].

Working with too high temperatures will deteriorate the winding insulation and the transformer oil, which are two aspects in which the lifespan of a transformer is very dependent [3]. This way it is very important to ensure an effective cooling system, especially in situations where high power is involved.

Transformers usually use oil and air as internal and external cooling mediums, respectively. When using oil, the coils and core are immersed in an oil filled tank. In small transformers, the tank surface in contact with the exterior air is enough to provide the heat dissipation needed. In larger transformers, since there is more heat generated, it is required that the oil circulates from the transformer's tank to external heat exchangers [2]. In Figure 2, it can be seen a power transformer with external radiators attached.

Figure 2 – Efacec's Power Transformer with radiators attached [1].

The oil and air circulation can be forced by mechanisms such as pumps and fans, respectively, or can be driven by natural buoyance forces. Having these circulation regimes, there will be forced and natural convection that can be combined together (for example the oil can be driven naturally and air forced by fans).

1.3. Project Description and Objectives

One of the five targets that European Union established for 2020 concerns the climate changes and the energy sustainability, more particularly an increase of 20% in energy efficiency [4]. Regarding transformers, although they are optimized in terms of the electric conversion process, there is still a lot of work that can be done in the cooling procedures. The optimization of transformer's cooling capacity allows the utilization of more compact equipment and consequently the reduction in manufacturing materials.

Several researches and improvements have been performed in the interior of transformers for enhance heat dissipation, being the analysis of the external heat exchangers less explored. These apparatus are a fundamental component for dissipating the heat generated into the exterior of a transformer. The capability of predicting the behaviour and cooling capacity of heat exchangers leads to a better and more adequate

selection of equipment for each particular transformer. This knowledge would allow the completion of a global system for designing transformers and also can lead to modifications in heat exchangers configurations in order to enhance their cooling capacity.

Consequently, the aim of this project is to develop and evaluate calculation methods to predict the cooling capacity of a type of heat exchangers applied in transformers: vertical plate radiators. These predictions should be based on the selection of the known input data (such as the oil inlet temperature, radiator characteristics, etc.) and on the calculation of the output parameters that are essentially the cooling capacity and the oil outlet temperature. In Figure 3 is a scheme of oil cooling in a vertical plate radiator and in Figure 4 is a diagram of the main calculation inputs and outputs.

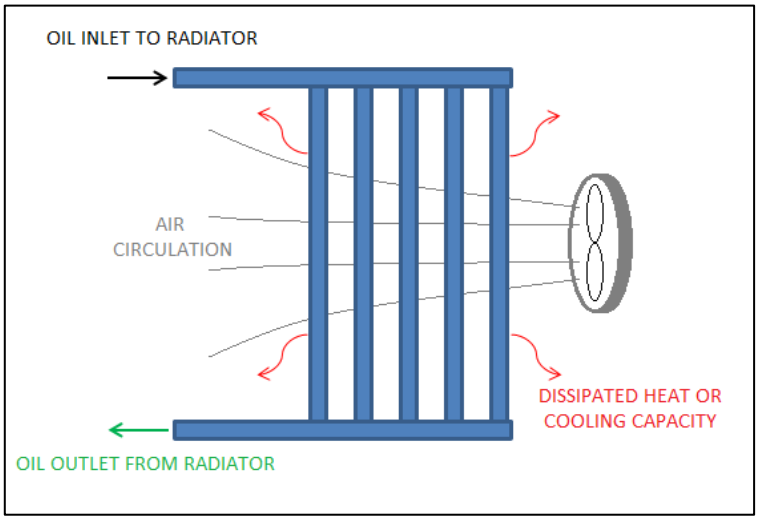

Figure 3 – Scheme of oil cooling in radiator.

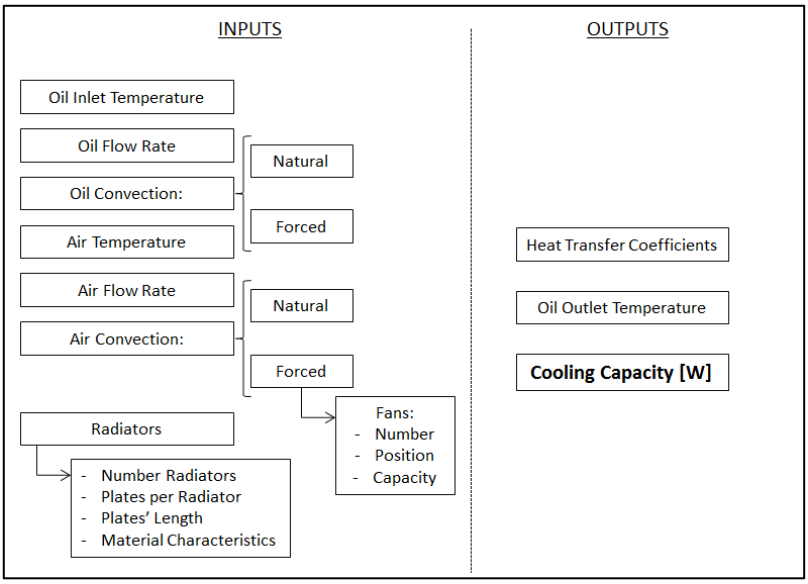

Figure 4 – Calculation inputs and outputs.

The mathematical model to be developed in this work is based on the utilization of heat transfer correlations. These correlations use dimensionless numbers (such as Reynolds, Rayleigh, Prandtl and Nusselt numbers), which in turn are calculated using the properties of the fluids. This implies the utilization of iteration procedures, for

example the oil outlet temperature has an initial arbitrated value that is corrected by progressive iterations.

Although results from experiments or CFD simulations can be more accurate than calculation methods, the last one is a much faster and less expensive tool. Using experimental apparatus to study every new configuration that appears would imply an unfeasible cost and time. With simulation tools the time problem would still remain if one wanted to study every single case.

In order to improve the calculation methodology, the existing correlations on literature (for natural and forced convection) were studied and the results will be compared with other sources in order to analyse the applicability of the correlations. Also, for the air forced convection, some correlations were developed using CFD simulations.

1.4. Structure and Organization

The text that follows the introduction is organized in four chapters. The first of these chapters is the *Background*, where the nomenclature of the transformer cooling states is presented, followed by the description of the type of radiators studied in this work. The state of the art is presented at the last section of the *Background*, concerning studies on vertical plate radiators by CFD simulations and experiments.

In chapter 3, the heat transfer modes on radiators are analysed. After this analysis, the calculation procedures are presented with the respective assumptions and then the methodology used to perform CFD simulations of air forced convection is described. Preliminary experiments were conducted for air natural convection and are described in the last section of chapter 3.

Chapter 4 contains the results and discussion divided into two sections: air forced convection and air natural convection. For the forced convection, the results from CFD simulations and its comparison with the calculation methodology using literature correlations are presented. Then the formulation of new correlations based on CFD results is shown, followed by a comparison between ventilate radiators with fans on the side and on the bottom. The subsection *Transformer 546A in ONAF* presents a comparison between the calculation procedures applied in a real transformer from Efacec and data from operational tests performed by the company in the same transformer.

For natural convection, the literature correlations were evaluated applying them in three case studies: the preliminary experiments performed, a transformer from Efacec and the experiments conducted by [5].

In the last chapter the final conclusions are presented and future work is recommended.

2. Background

In this chapter, a background for the transformers external heat exchangers is presented. A transformer can operate at different cooling states, which designation depends on the cooling mediums used and their circulation mechanisms. The nomenclature of the cooling states is presented in the first section. In the second section the vertical plate radiators are described along with their geometrical characteristics and main configurations. The state of art on the performance of the radiators is presented on the last section of this chapter.

2.1. Transformer Cooling States

There are several cooling states used for the refrigeration of power transformers and therefore transformers shall be identified according to the applied method. According to the *International Electrotechnical Commission* (IEC), for the case of liquid-immersed transformer, the cooling state is identified by a four letter code. The first letter relates to the internal cooling medium and the second regards to its circulation mechanism. The third and fourth letters are associated to the external cooling medium and its circulation mechanism, respectively. The existing letters and their meaning can be seen in Table 1 [6].

Table 1 - Four letter code to identify transformer's cooling state [6]

Order	Letter	Meaning
First	O	Mineral oil or synthetic insulating liquid with fire point less or equal to 300ºC.
	K	Insulating liquid with fire point over 300ºC.
	L	Insulating liquid with no measurable fire point.
Second	N	Natural thermosiphon flow through cooling equipment and in windings.
	F	Forced circulation through cooling equipment, thermosiphon flow in windings.
	D	Forced circulation through cooling equipment, directed from the cooling equipment into at least the main windings.
Third	A	Air
	W	Water
Fourth	N	Natural convection.
	F	Forced circulation (fans or pumps).

A transformer can have alternative cooling states. For example, an ONAN/ONAF has a set of fans which may be put into service at high loading [6].

Along this project, four types of cooling states were studied:

- ONAN – Oil Natural Air Natural
- ODAN – Oil Directed Air Natural
- ONAF – Oil Natural Air Forced
- ODAF – Oil Directed Air Forced

Oil immersion is commonly used because this cooling medium has higher dielectric strength than air and that is fundamental to prevent electric breakdown or discharge at the coils and core of the transformer [2]. Therefore it is not possible to choose the internal cooling medium attending only to its cooling capacity, since it works also as an electrical insulator.

The typical oils used in transformers are the mineral type ones. Mineral oils provide efficient cooling and electrical insulation, but they have low biodegradability. Due to this inconvenience, the main research that is being carried out has the aim of finding other fluids that are biodegradable (like vegetable oil-based and synthetic esters) and still have the required properties for operation. This kind of research and testing can be found in [7] and [8].

Air is frequently chosen to be the external cooling medium, since it doesn't involve acquisition costs and its return to the environment doesn't require special attention. The same may not be true when using water.

Systems based on oil and air natural flows (ONAN – Oil Natural Air Natural) are the most reliable ones, since there aren't any mechanical components, like pumps or fans, which can fail. This type of systems are absent of mechanical vibration and noise [5] and their simplicity makes them economically interesting. On the other hand, forced circulation of the cooling mediums brings more efficiency and from there results greater cooling capacities and/or more compact equipment.

2.2. Vertical Plate Radiators

The typical heat exchangers used in power transformers consists in thin vertical plate radiators. Figure 5, shows an example of this type of heat exchangers. There is a great interest in using these radiators due to their construction simplicity that makes them more economically sustainable.

Figure 5 - Vertical Plate Radiators [9].

A scheme of the oil circuit can be seen in Figure 6. The oil comes from the transformer's tank from the inlet pipes and enters in the radiator plates at their top. After

passing through the plates, the oil re-enters the tank through the outlet pipes located in the bottom part of the radiators. At the external surface of the plates circulates air at room temperature, driven by natural or forced circulation (for this last one are used coupled fans).

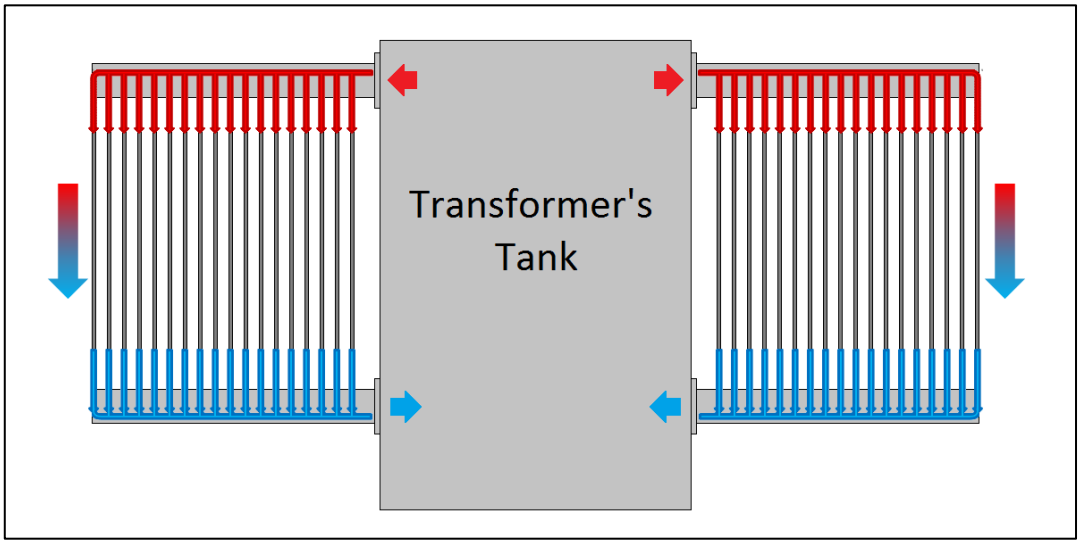

Figure 6 – Oil circulation scheme.

Presently, the cooling capacity of the radiators is estimated using tabulated experimental information and some correction factors are applied. There are several parameters that affect the cooling capacity and some of them are not taken into account in that method. The main geometrical parameters are presented in Table 2 and Figure 7.

Table 2 – Radiators geometrical parameters

Geometrical Parameter	Range or Standard Values
Distance Between Plates - S	45 mm
Plate Width - W	520 mm
Plate Length - L	800 to 3500 mm

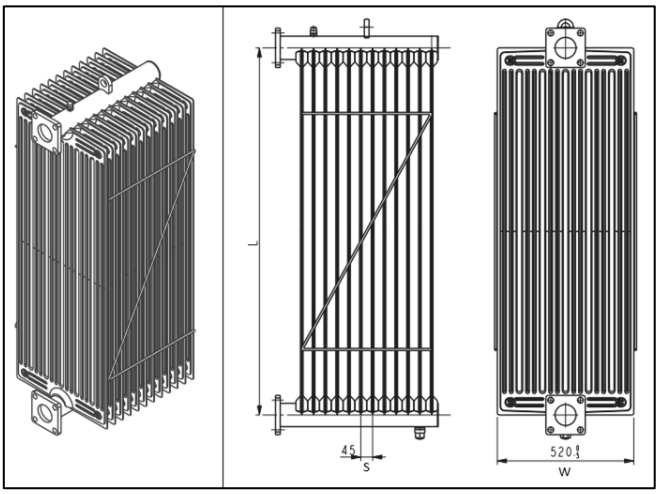

Figure 7 – Radiator and main dimensions. Adapted from [10].

The plates are evenly separated and all have the same width, but in the same radiator can be present plates of different lengths. Each plate has six oil channels. In Figure 8 is presented the geometry and dimensions of an oil channel cross section. This geometry was designed in *SolidWorks* (Figure 9) in order to easily estimate values of areas and perimeters.

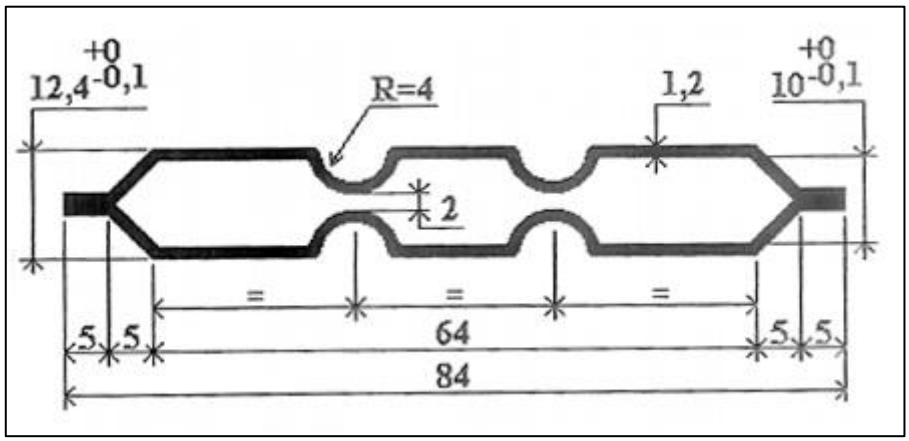

Figure 8 – Oil channel cross section dimensions. [11]

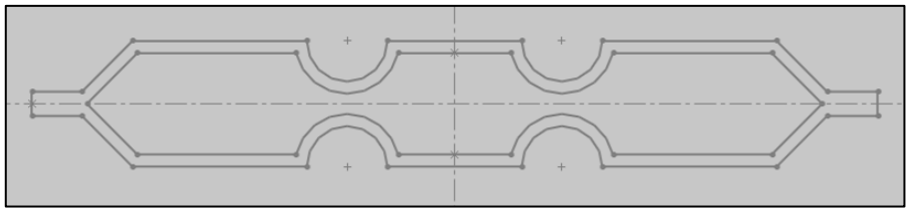

Figure 9 – Oil channel cross section designed in *SolidWorks* software.

In order to predict the cooling capacity provided by the radiators installed in a transformer and also the oil temperature at the radiators' outlet, it is necessary to consider other parameters beside the geometrical ones. Such parameters include:

- The oil flow rate;
- The air flow rate;
- The oil temperature at the radiator's inlet;
- The air temperature;
- The properties of the cooling mediums (oil and air);
- The properties of the radiators' material;
- Number of radiators;
- Number of plates per radiator;
- Fans position and distribution.

There are several configurations for the position of the fans. In general terms, fans can be located at the bottom or at the side of the radiators. For the later case, the radiators can be disposed in groups, being each group cooled by a set of fans (fan bank). These two types of positioning are shown in Figure 10 (bottom ventilation) and in Figure 11 (side ventilation).

Figure 10 – Radiators cooled with fans on the bottom [12].

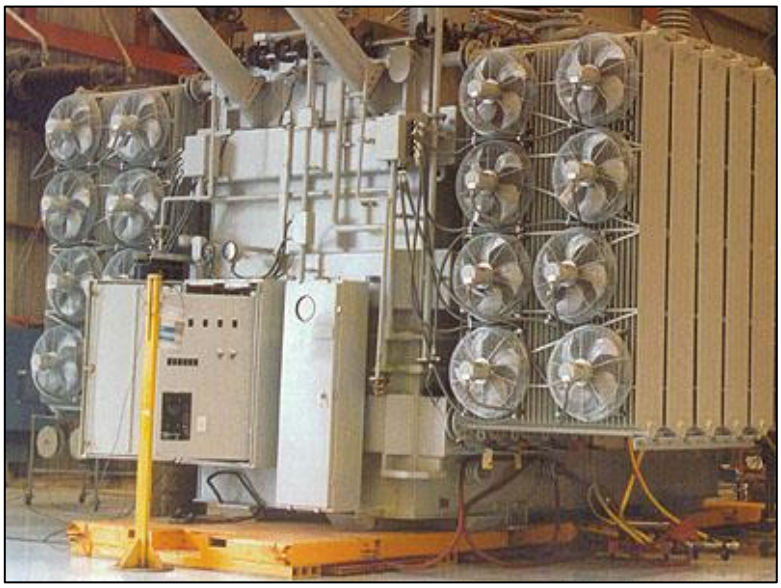

Figure 11 – Group of radiators cooled by lateral set of fans [13].

Each configuration requires special considerations, like considering a counter or a cross flow arrangement and considering the loss in air velocity by having more radiators to a fan bank.

Note that the parameters used in forced and natural convection are different. For example, in air natural convection the air flow rate is unknown.

2.3. State of Art

In this section is presented the reviewed literature related with vertical plate radiators research. The described literature includes CFD simulation analyses, experimental results and theoretical calculations.

As stated before, the interior of transformers have been widely studied but only a few reports were found with focus on the radiators. Nabati and Mahmoudi [14, 15]

studied, by means of CFD simulation, the oil flow and heat transfer of a power transformer radiator. Experimental data was taken, for verification of the results, from Iran Transfo Company. In [14] they considered a single radiator element and have modelled one quarter of it based on symmetrical properties. The surface shape of the radiator plate was modelled with detail as it can be seen in the left side of Figure 12.

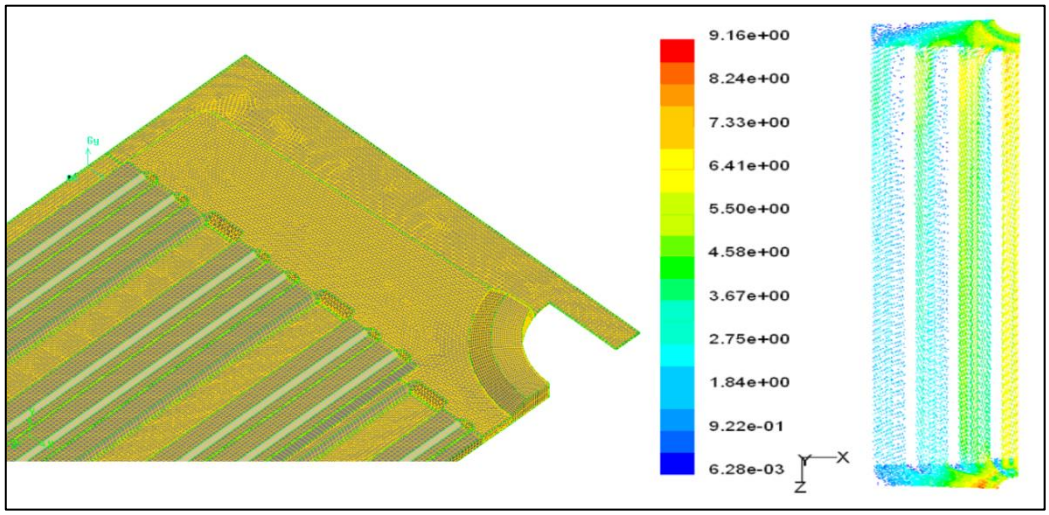

Figure 12 – Radiator surface shape (left) and oil velocity vectors (right) [14].

Both ONAN and ONAF states were simulated with this model and the authors concluded that the oil flow passage needs some correction since the oil mass flow distribution is not homogenous (right side of Figure 12). They reported that the velocity magnitude in the outer passages is half of the middle one, which decreases the heat transfer coefficient and the radiator cooling efficiency.

The same authors in [15] modelled a radiator block with 18 plates and conducted simulations for ONAN state. The radiator elements were modelled as a rectangular cube shape and inlet and outlet pipes were included. They conclude from the temperature distribution that there were some dead zones resulting from recirculation flows. They also reported that small amount of inlet flow reached the plates more distant from the inlet, as it can be seen in Figure 13. As a consequence of this maldistribution there is a big difference in the heat transfer efficiency of the first and last plates.

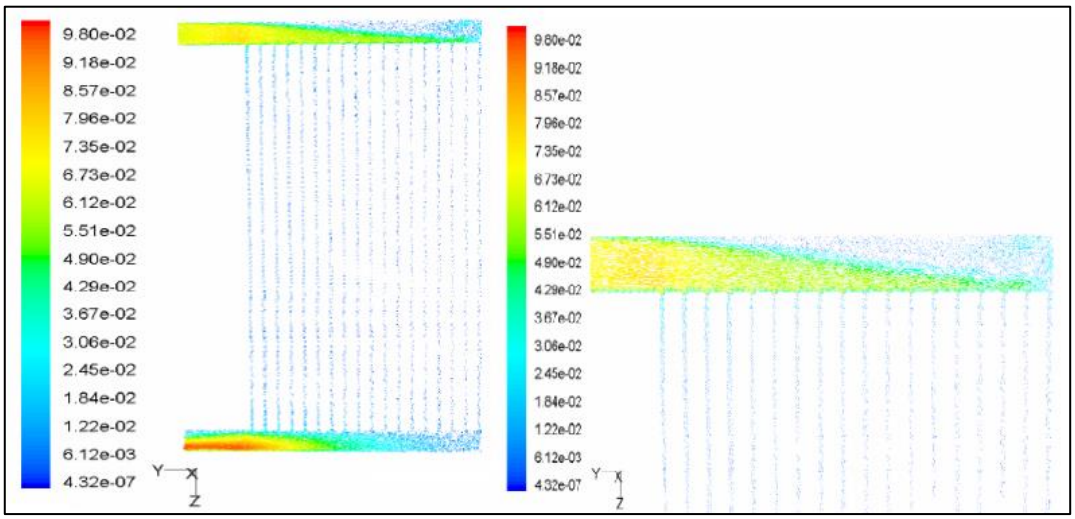

Figure 13 – Velocity vectors in the middle section of block [15].

In both papers [14] and [15], the air heat transfer convection was not modelled since the heat transfer coefficient was calculated theoretically and then introduced in the simulation as input data. It is commented in [15] that numerical results of cooling capacity revealed a difference of about 15% from technical data and that could be a result from considering a constant convection coefficient for all radiators.

Also in both papers, buoyance effect was assumed negligible inside the radiator and heat transfer by radiation was not considered. The buoyancy force was calculated previously to simulation and its value was introduced as a boundary condition.

Min-gu Kim et al. [5] performed a study on the cooling performance of transformer radiators in the ONAN and ODAN states, supported by the Hyosung Corporation. An arrangement of four radiators was evaluated, having each radiator 40 plates spaced of 45mm and with 3300mm length. Theoretical calculations and CFD simulations were performed in order to predict the cooling capacity of the arrangement. The results provided by these two methods were compared with experimental data. The experimental apparatus used is shown in Figure 14.

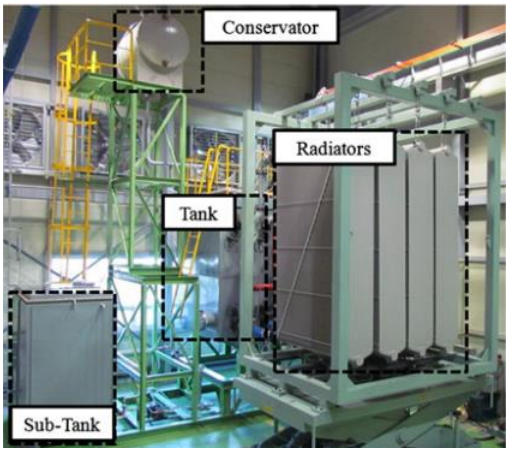

Figure 14 – Experimental setup installation used on [5].

Three experiments were performed, one of them with oil flow thermally driven (ON – Oil Natural) and in the other two the oil was pumped with different flow rates (OD – Oil Directed). Since no fans were used (AN - Air Natural), the experiments were made in ONAN and ODAN.

Regarding the theoretical calculations, empirical correlations were used to determine the air convective heat transfer coefficients. For the outer plates was used a correlation that considers vertical isolated flat plates:

$$Nu_L = \frac{h \cdot L}{k} = \left[0.825 + \frac{0.387 \cdot Ra_L^{1/6}}{\left(1+(0.492/Pr)^{9/16}\right)^{8/27}}\right]^2 \tag{2.1}$$

For the inner plates it was employed an equation for flat, parallel and symmetric plates with a small ratio between the plates' spacing and length:

$$Nu_S = \frac{h \cdot S}{k} = \frac{1}{24} \cdot Ra_S \cdot \left(\frac{S}{L}\right) \cdot \left[1 - \exp\left(-\frac{35}{Ra_S \cdot (S/L)}\right)\right]^{3/4} \tag{2.2}$$

The application of equation 2.2 was based on the assumption that the flow between plates is fully developed with merged boundary layers.

In equations 2.1 and 2.2, *Nu*, *Pr* and *Ra* are the Nusselt, Prandtl and Rayleigh numbers, respectively. The letters *h*, *k*, *S* and *L* stand for the air heat transfer coefficient, its thermal conductivity, the space between plates and the plate length, respectively. It is important to refer that the oil flow rate distribution between plates was estimated using an equation (equation 2.3) obtained from CFD tool (*Fluent v.13*).

$$Q_{oil}(N) = (1.409 - 0.031N + 0.000416N^2)\left(\frac{Q_{total}}{N_{total}}\right) \quad (2.3)$$

Where $Q_{oil}(N)$, N, Q_{total} and N_{total} are respectively the oil flow rate in plate N, the order of the plate, the total oil flow in radiator's inlet and the total number of plates.

In the CFD simulations one radiator was modelled reflecting the real shape of its surfaces and considering the internal oil flow and the external convection with the surrounding ambient air. One of the temperature distributions obtained is showed in Figure 15.

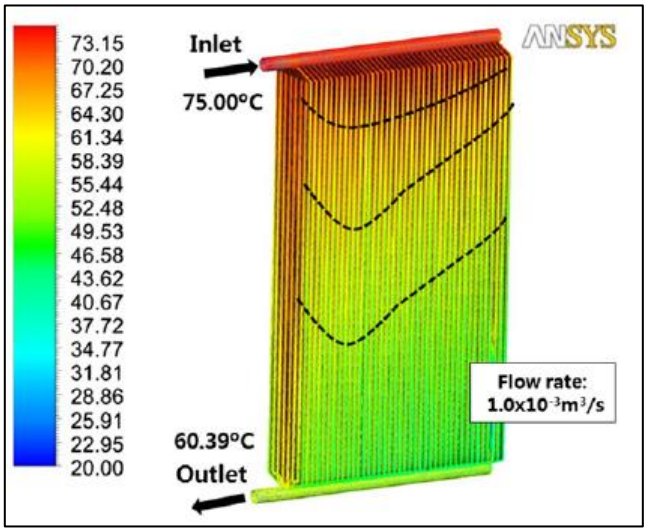

Figure 15 – Radiator temperature distribution obtained in CFD simulation [5].

Figure 16 shows the comparison between the cooling capacity from experimental results, CFD simulation and theoretical calculations.

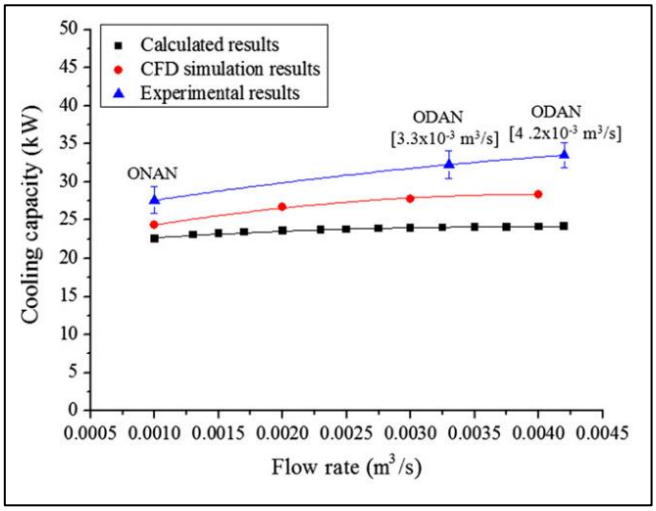

Figure 16 – Cooling capacity for different oil flow rates [5].

Average deviations of calculated results versus the CFD simulations and experiments are reported as 13.47% and 31.6%, respectively. The authors concluded that assuming vertical flat plates with constant temperature in calculations is the main cause for their deviation. It is reported an average deviation of 15.8% in the cooling capacity from CFD simulations versus the experimental results. The radiation effect was not considered in these simulations and the authors attribute this as the cause of the difference from experimental results.

A different study performed by Fdhila et al. [16], supported by ABB Corporate Research, was made on radiators cooling capacity in the ONAF state. They performed CFD simulations using a porous medium approach to model the mixed convection between oil and air flows in the radiators and using a standard turbulent heat transfer model to the air surrounding the radiators. A specific transformer has been chosen to perform this analysis. This transformer and its CFD model geometry can be seen in Figure 17, in the left and right sides respectively.

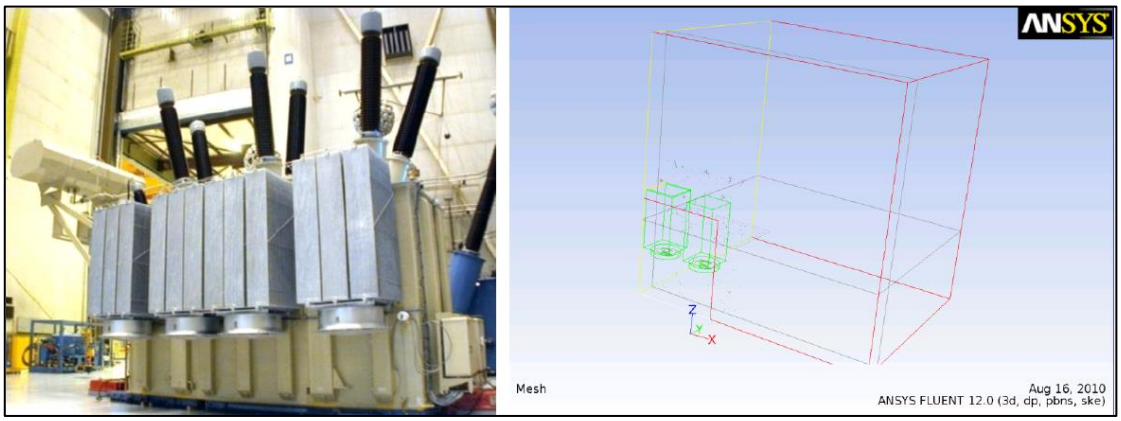

Figure 17 – Reference transformer (left) and corresponding CFD model geometry (right) [16].

The heat transfer from oil to air was modelled with a common heat transfer coefficient, but in order to represent the radiators parallel plate structure, the porous medium was defined as anisotropic.

A fine and accurate grid is used in the porous medium (radiators), a much coarser one is used in the outside air and an intermediate grid is present in between. A horizontal cross-cut of these grids can be seen in Figure 18.

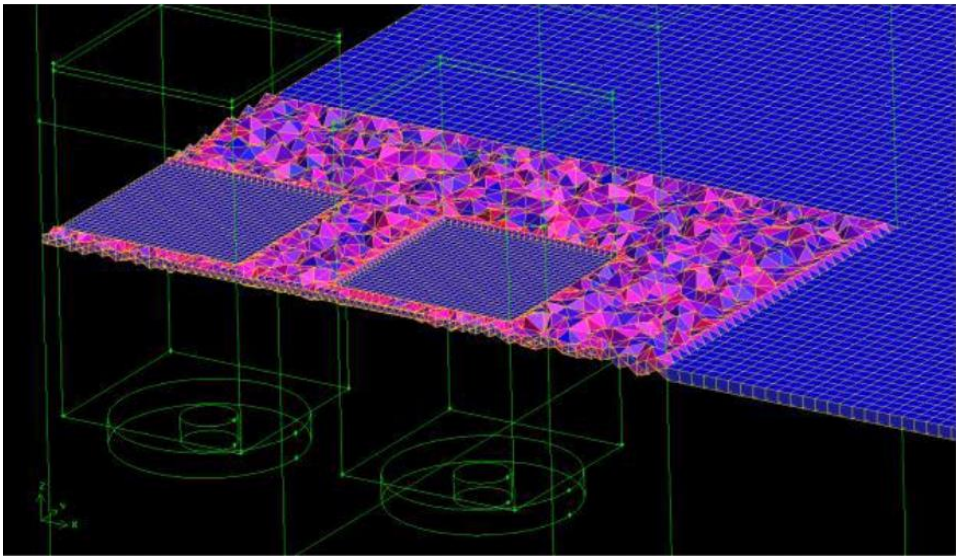

Figure 18 – Horizontal cross-cut of computational grid [16].

According to the authors this CFD model provides a fast and accurate approach for performing realistic simulations.

As domain boundaries this model has the floor, the transformer tank wall (simulated as adiabatic) and open domain boundaries located far away from radiators. The oil flow rate and inlet temperature were fixed and the fans were modelled as volumes with known velocity in the boundary.

Since smaller fans allow a better coverage of the radiator inlet area, the impact in cooling capacity of using a larger number of smaller fans was investigated, maintaining the total air flow. The fans diameter was varied from 0.8 to 1.5m and arrangements of two, three and four fans were simulated. In the case of the three fans arrangement, two different configurations were considered. The results can be seen in Figure 19.

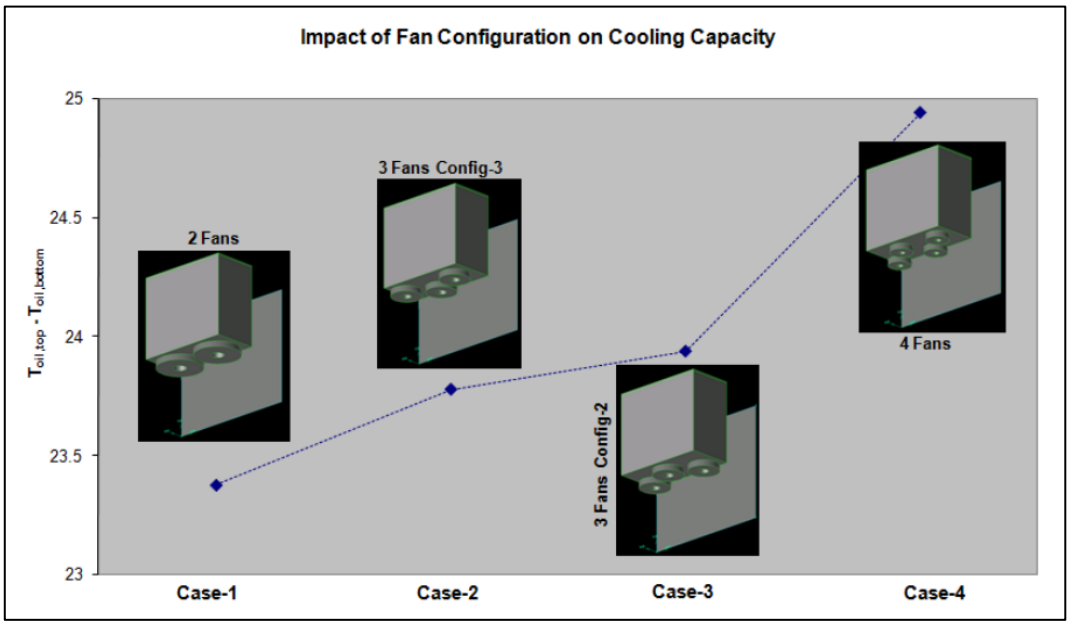

Figure 19 - Top-to-bottom oil temperature difference for four fan configurations [16].

The authors reported that the cooling capacity increases if the same amount of air is spread with smaller fans and also concluded that the transformer tank wall has

some influence on cooling capacity since the different configurations with three fans have the same result.

Overviewing the state of art, there have been made interesting studies in vertical plate radiators performance but a lot of parameters have to be studied to fully understand the effect of radiators' configurations in the cooling capacity. The simulations made on papers [14] and [15] focus on oil flow distribution and [16] on the air distribution and resulting cooling capacities, not being an objective of these works to find a theoretical calculation methodology to predict radiators performance. An evaluation of using heat transfer correlations is performed on [5] in a very complete approach, but air forced convection was not explored and radiation was neglected. Also the oil thermal resistance was not considered in calculations and it can have importance in the total heat transfer process. The difference of calculated and experimental results is considerable and maybe a better look at the air convection phenomenon could be useful for finding a new correlation that adjusts better to the radiators case.

3. Modelling of Heat Exchangers

The heat exchangers presented previously have been modelled for two different objectives: development of a calculation methodology and development of CFD simulation model, both for predicting the heat exchangers performance. These two models are described in this chapter along with the assumptions that were considered. The calculation methodology considers all cooling states but the CFD simulations were conducted only for air forced convection (AF). Before describing the calculation procedures and the simulations, an analysis is presented about the heat transfer modes that occur in the radiators' plates.

In the last section of this chapter are presented the details of two preliminary experiments that were conducted in an experimental facility of Efacec. These experiments were performed in the ODAN cooling state.

3.1. Heat Transfer Modes Analysis – AN and AF

Whenever a temperature difference exists in a medium or between media, heat transfer must occur [17]. There are three types of heat transfer modes:

- Conduction: when temperature gradient exists in a stationary medium;
- Convection: when a surface and a moving fluid are at different temperatures;
- Radiation: All surfaces of finite temperature emit energy in the form of electromagnetic waves.

In a radiator plate there are two moving fluids (oil and air) and a solid between them (the steel sheet that forms the plate). Taking into account the heat transfer modes, it is easy to identify that in oil heat is transferred by convection to the internal surface, then conducted in the steel sheet and transferred from the external surface to the air by convection again. A scheme of the heat transfer modes in a plate is shown in Figure 20, with the associated thermal resistances represented.

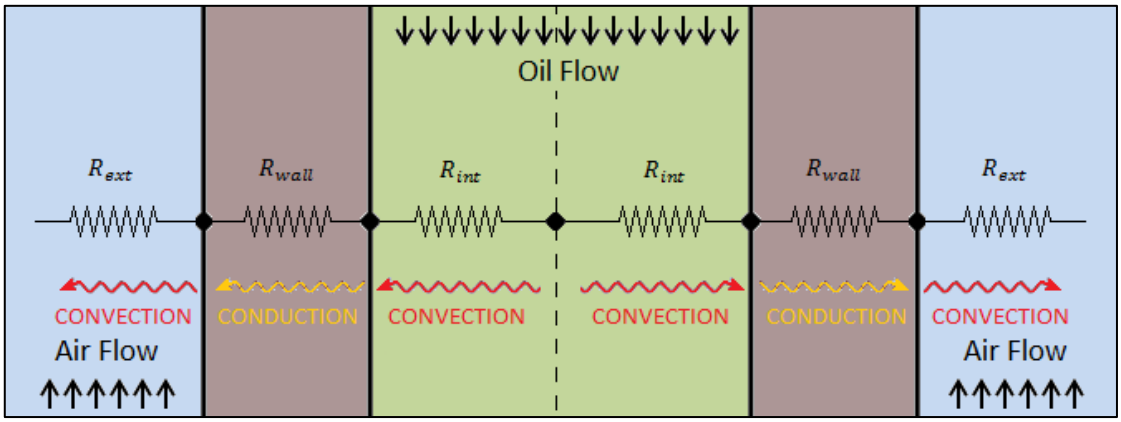

Figure 20 – Scheme of thermal modes in a plate and thermal resistances analogy.

The radiation mode is not included yet, but since this mode requires more complex calculus, a simple estimative can be made using the other modes to know the weight of each thermal resistance in the heat transfer process. In order to evaluate the

contribution of each mode in different cooling states, data from two real transformers (Efacec transformers) was taken and can be seen in Table 3.

Table 3 - Data from two transformers, each one in two different cooling states

Transformer Reference	**546 A**		**767 A**	
Number of Radiators	12		18	
Plates per Radiator	18		28	
Plates Length [mm]	3 of 1800 15 of 2200 (per radiator)		All with 3200	
Cooling State	**ONAN**	**ONAF**	**ODAN**	**ODAF**
$\mathbf{T_{oil;in}}$ **[ºC]**	60.3	53	57	57
$\mathbf{T_{air;in}}$ **[ºC]**	23.5	26	19	19
$\mathbf{Q_{oil;transformer}[m^3/h]}$	16.8	16.1	330	330
$\mathbf{Q_{air;fan}[m^3/h]}$	-	4400	-	10200
Fans per Radiator	-	4	-	4
Fans Position	-	Side	-	Side

With this information and using correlations for oil and air, for natural and forced convections, the thermal resistances were obtained. More information about this calculation procedures are going to be presented in the next section.

In Table 4 is shown the percentual weight of the thermal resistances in the different cooling states.

Table 4 – Thermal resistances of heat transfer modes in percentual weight, for four cooling states

Cooling State	**ONAN**	**ONAF**	**ODAN**	**ODAF**
$\mathbf{\%R_{int}}$	6.19%	21.01%	5.76%	22.44%
$\mathbf{\%R_{wall}}$	0.02%	0.08%	0.02%	0.08%
$\mathbf{\%R_{ext}}$	93.79%	78.91%	94.22%	77.48%

As it can be seen from Table 4, the thermal resistance of heat conduction in the plate walls has a very low weight in all cooling states (maximum of 0.08%). Therefore, in order to simplify the calculation procedure, this resistance will be neglected and the temperatures of the wall in the internal and external sides will be considered equal.

It is also important to notice that the thermal resistance in oil should not be neglected since the results show that it contributes considerably in the heat transfer process, especially if the fans are turned on (ONAF and ODAF states). This happens because the increase in air velocity reduces its thermal resistance, while the oil convection resistance remains the same increasing its relative weight.

3.2. Calculation Procedures – AN and AF

Reviewing some literature in heat transfer it was found that forced convection is much more explored then natural convection and more Nusselt correlations for different geometries are available in forced convection. It appears to be easier to model forced convection, since the fluid flow is imposed and consequently the flow rate and/or the fluid's velocity typically are known. The same doesn't happen in natural convection because fluid's motion results from buoyance forces caused by temperature gradients. Knowing the value of fluids' flow rate is very useful in heat transfer to calculate the cooling capacities and fluids temperature at the end of the heat exchange.

In a transformer, buoyance forces that induce oil movement are generated by the thermal gradients in the tank and in the radiators. Since the tank has greater volume than the radiators, it is going to be assumed that the major contribute in oil motion is given by the tank's thermal gradients and so its convection will be treated in radiators as a forced one. The values of oil flow rate in natural convection are taken from a simulation tool for the tanks of transformers developed by Efacec.

As a consequence of this assumption, the oil flow rate was always an input data in the following calculation procedures and forced convection correlations were used. Thus OD and ON states have the same considerations in calculation methodology.

Concerning the air flow, forced and natural convection correlations are employed when fans are turned on and off, respectively.

In the next subsection oil convection analysis is going to be presented first and its considerations are valid for all cooling states. After that, air natural convection procedures are stated, completing the methodology for ONAN and ODAN states, and then air forced convection is considered, concluding ONAF and ODAF states. Finally in the last subsection is presented the methodology used to include the radiation effect in calculations.

3.2.1. Convective Heat Transfer Inside the Oil

In order to estimate the cooling capacity of the radiators, convective heat transfer coefficients for oil and air have to be calculated. As previously stated, the oil flows through a plate being divided in six identical channels. Using the design information in [11] and *Solidworks* software, the internal and external perimeters of each channel were estimated. The internal cross section of a channel and the external perimeter of the entire plate were also calculated (these values are constant because the plate width is always the same). These values are presented in Table 5.

Table 5 – Evaluation of some constant geometric parameters of a plate

Channel Internal Perimeter	$0.1695\ m$
Plate External Perimeter	$1.2041\ m$
$\mathbf{A_{cross;channel}}$	$5.5963 \times 10^{-4}\ m^2$

With these values is possible to determine the heat transfer areas as well as the channel hydraulic diameter using equations 3.1 to 3.3.

$$A_{int} = 1.017 \cdot L \tag{3.1}$$

$$A_{ext} = 1.2041 \cdot L \tag{3.2}$$

$$D_{h;channel} = \frac{4 \cdot A_{cross;channel}}{Channel\ Internal\ Perimeter} = 0.0132m \tag{3.3}$$

Where A_{int}, A_{ext}, $D_{h;channel}$ and L are the plate total internal area, the plate external area, the channel hydraulic diameter and the plate length, respectively.

The oil flow regime was evaluated with the Reynolds number using the channel hydraulic diameter (equation 3.4), since it is an internal flow.

$$Re_{D;oil} = \frac{\rho_{oil} \cdot (Q_{oil;channel}/A_{cross;channel}) \cdot D_{h;channel}}{\mu_{oil}} \tag{3.4}$$

Where ρ_{oil} and μ_{oil} are oil's density and dynamic viscosity calculated at the oil average temperature [17]. The $Q_{oil;channel}$ is the oil flow rate in a channel and it was estimated considering that the oil flow is distributed equally by all plates and all channels.

In all studied cases, $Re_{D;oil}$ was found to be much smaller than 2300, which means the flow is laminar. According to [17], for laminar and fully developed flows the Nusselt number can be obtained consulting the information in Figure 21.

Cross Section	$\frac{b}{a}$	$Nu_D = \frac{hD_h}{k}$ (Uniform q_s'')	$Nu_D = \frac{hD_h}{k}$ (Uniform T_s)	Re_{D_h}
	—	4.36	3.66	64
	1.0	3.61	2.98	57
	1.43	3.73	3.08	59
	2.0	4.12	3.39	62
	3.0	4.79	3.96	69
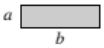	4.0	5.33	4.44	73
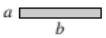	8.0	6.49	5.60	82
 Heated	∞	8.23	7.54	96
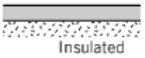 Insulated	∞	5.39	4.86	96
	—	3.11	2.49	53

Figure 21 – Nusselt numbers for fully developed laminar flow in tubes of different cross section [17].

The fully developed conditions were verified using equation 3.5 (where x_{fd} is the hydrodynamic entry length [17]) and the ratio b/a was estimated in approximately 7. Taking this into account and considering a uniform wall temperature condition, the Nusselt number is 5.60 (equation 3.6).

$$x_{fd} \approx 0.05 \cdot Re_{D;oil} \cdot D_{h;channel} \tag{3.5}$$

$$Nu_{D;oil} = 5.60 \tag{3.6}$$

To determine the oil heat transfer coefficient in one channel, equation 3.7 was used. With this value and knowing the channel heat transfer area (1/6 of the total internal area), the channel thermal resistance can be obtained using 3.8.

$$h_{channel} = Nu_{D;oil} \cdot \frac{k_{oil}}{D_{h;channel}} \tag{3.7}$$

$$R_{channel} = \frac{1}{h_{channel} \cdot \frac{A_{int}}{6}} = \frac{6}{h_{channel} \cdot A_{int}} \tag{3.8}$$

Where $h_{channel}$, k_{oil} and $R_{channel}$ are the channel internal heat transfer coefficient, the oil thermal conductivity and the channel thermal resistance. Since there are 6 channels in a plate, by the electric resistances analogy this corresponds to 6 equal resistances in parallel and the total plate internal thermic resistance (R_{int}) can be obtained with equation 3.9.

$$R_{int} = \frac{R_{channel}}{6} = \frac{1}{h_{channel} \cdot A_{int}} \tag{3.9}$$

Notice that all oil properties values are considered at the fluid's average temperature since this is an internal flow. These values are calculated with equations that are function of temperature, being this equations extracted from company's charts (Annex A).

3.2.2. ONAN and ODAN states

The heat transfer process from oil to air can be seen as a series of two thermal resistances system, with the oil temperature in one side and the air temperature in the other. This is illustrated in Figure 22.

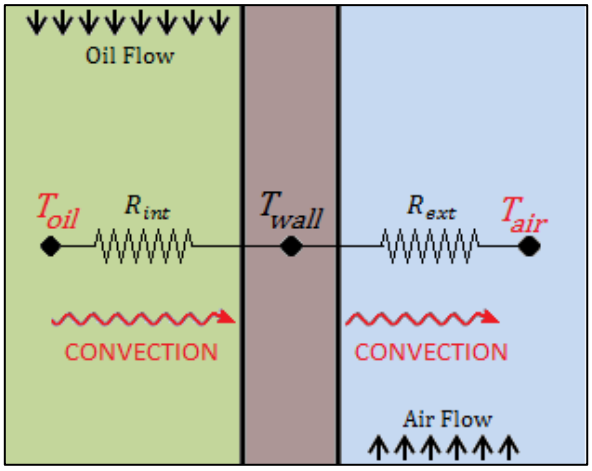

Figure 22 – Heat transfer as a series of thermal resistances.

The heat dissipation can be calculated with equation 3.10:

$$P_{plate} = \frac{T_{oil;ave} - T_{air}}{R_{int} + R_{ext}} \tag{3.10}$$

Where P_{plate}, $T_{oil;ave}$, T_{air} and R_{ext} are respectively the plate heat dissipation (in watts), the oil average temperature, the air room temperature and the plate external

thermal resistance. Notice that the air temperature used is not the average between inlet and outlet because in this case air convection is natural and so this values are not known as well as the air flow rate.

To calculate R_{ext} is required the air convection coefficient. This coefficient may be different at the inner and outer surfaces. In order to differentiate these convection coefficients, the one for the inner surfaces was designated h_{gap} and the other h_{end}. In Figure 23 is a scheme of this nomenclature.

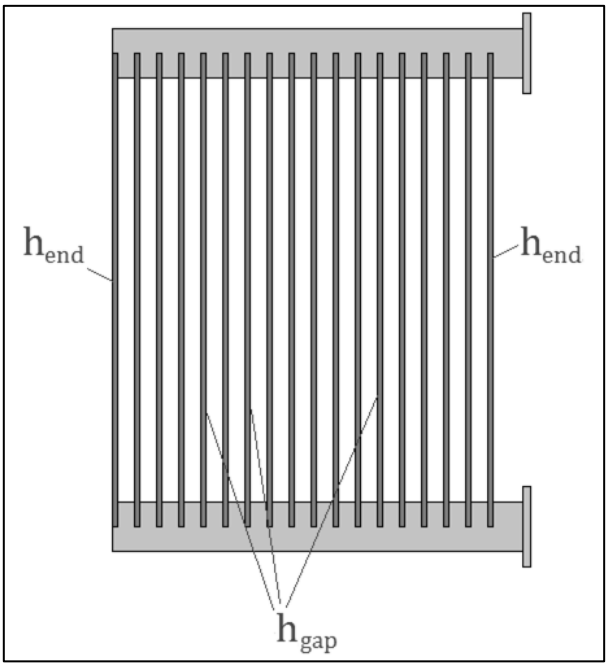

Figure 23 – Scheme of air convection coefficients nomenclature.

In this sequence there are two different external thermal resistances, R_{gap} and R_{end}, that were calculated using 3.11 and 3.12.

$$R_{gap} = \frac{1}{h_{gap} \cdot A_{ext}} \tag{3.11}$$

$$R_{end} = \frac{1}{h_{end} \cdot A_{ext}} \tag{3.12}$$

Notice that in equations 3.1 and 3.2, the internal and external areas were calculated with the plate's perimeter and so these areas as well as the thermal resistances regard both sides of a plate. The total cooling capacity of a radiator was obtained using equations (3.13) to (3.15).

$$P_{gap} = \frac{T_{oil;ave} - T_{air}}{R_{int} + R_{gap}} \tag{3.13}$$

$$P_{ends} = \frac{T_{oil;ave} - T_{air}}{R_{int} + R_{end}} \tag{3.14}$$

$$P_{radiator} = (N - 1) \cdot P_{gap} + P_{ends} \tag{3.15}$$

Where $P_{radiator}$ is the radiator's cooling capacity and P_{gap}, P_{ends} and N are respectively the heat dissipated between two plates, the heat dissipated through the surfaces at the ends and the number of plates present in the radiator.

The coefficient h_{end} was calculated using a Nusselt correlation for isolated vertical plates developed by Churchill and Chu [18] for laminar and turbulent natural convection. This correlation is shown in equation 3.16 and in 3.17 is the Rayleigh number that was used.

$$Nu_L = \frac{h_{end} \cdot L}{k_{air}} = \left[0.825 + \frac{0.387 \cdot Ra_L^{1/6}}{\left(1+(0.492/Pr)^{9/16}\right)^{8/27}}\right]^2 \quad (3.16)$$

$$Ra_L = \frac{g \cdot \beta_{air} \cdot (T_{wall} - T_{air}) \cdot L^3}{\nu_{air}^2} \cdot Pr \quad (3.17)$$

Where T_{wall} is the average surface temperature. Two hypotheses were made for the air convection between plates (Figure 24):

- The distance between plates is big enough so the thermal boundary layers don't overlap and each plate behaves as an isolated one.
- The thermal boundary layers overlap and so the air flow is developing between plates.

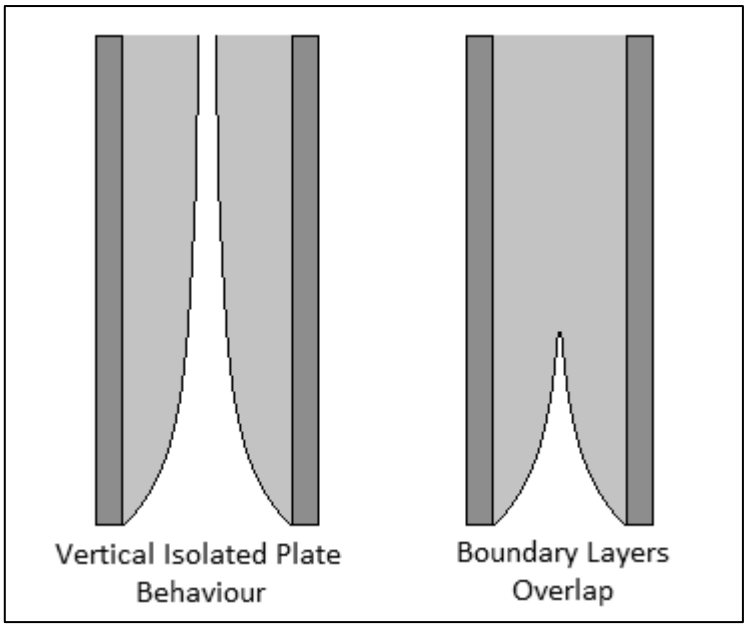

Figure 24 – Hypothesis for air convection between plates.

For the first hypothesis h_{gap} was calculated using the same correlation of h_{end}, equation 3.16. For the second hypothesis equation 3.18 was used to calculate h_{gap}. The Rayleigh number in this correlation is calculated using equation 3.19.

$$Nu_S = \frac{h_{gap} \cdot S}{k_{air}} = \frac{1}{24} \cdot Ra_S \cdot \frac{S}{L} \cdot \left[1 - \exp\left(-\frac{35}{Ra_S \cdot S/L}\right)\right]^{\frac{3}{4}} \quad (3.18)$$

$$Ra_S = \frac{g \cdot \beta_{air} \cdot (T_{wall} - T_{air}) \cdot S^3}{\nu_{air}^2} \cdot Pr \quad (3.19)$$

Equation 3.18 was proposed by Elenbaas in [19] for symmetrically heated isothermal plates. This correlation was formulated considering two limits of parallel plates' arrangement: $S \to 0$ and $S \to \infty$ (being S the distance between plates). When considering the second limit, the correlation was adjusted to match the values of a free vertical plate correlation. The correlation presented on equation 3.18 should be enough

to include both cases presented in Figure 24, the problem is that the free vertical plate correlation used in [19] is valid in the laminar regime. Since the obtained values of Rayleigh number in the current work indicate that the flow is turbulent, equation 3.16 was used to compare results. No correlation concerning natural convection in turbulent flows between parallel plates was found.

In natural convection all properties were evaluated at the film temperature:

$$T_{film} = \frac{T_s + T_{air}}{2} \tag{3.20}$$

In order to use the described methodology, the values of oil outlet temperature and surface temperature were initially arbitrated and then corrected, making iterations with equations 3.21 and 3.22 taken from the energy balance.

$$P_{radiator} = \rho_{oil} \cdot Q_{oil} \cdot c_{p_{oil}} \cdot (T_{oil;in} - T_{oil;out}) \tag{3.21}$$

$$\frac{P_{radiator}}{N} = \frac{1}{R_{int}} \cdot (T_{oil;ave} - T_{wall}) \tag{3.22}$$

The flowchart in Figure 25 summarizes the calculation procedure for ONAN and ODAN systems.

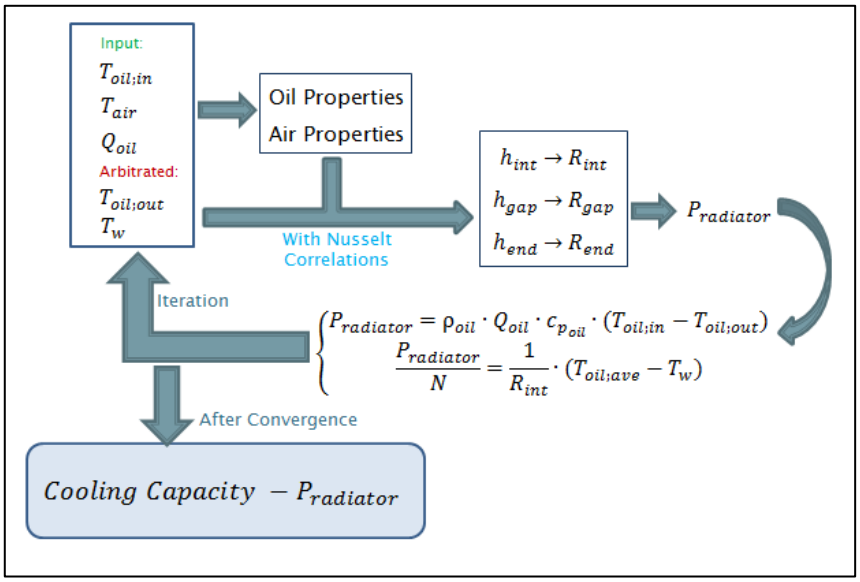

Figure 25 - Calculation Procedure for ONAN and ODAN states.

3.2.3. ONAF and ODAF states

The general calculation procedure for ONAF and ODAF states is very similar to the on for the previous cooling states, but the convective heat transfer coefficient is calculated in a different way. This coefficient was also considered different in the inner and outer plates, being named also h_{gap} and h_{end}, respectively.

Two different considerations could be made: the air flow from the fans goes through the gaps between plates and also goes to the outer surfaces or only between plates (Figure 26).

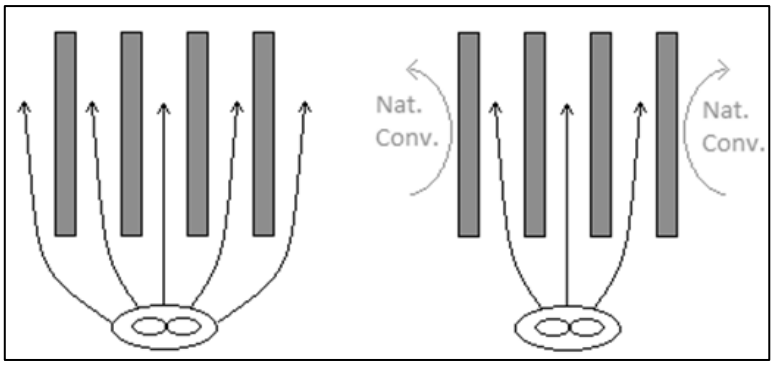

Figure 26 - Two possible flow paths for the air from the fans.

It was considered that the forced air flow is driven only between plates and at the outer surfaces only natural convection takes place. In the typical arrangements fans are very close to radiators and so a little quantity or even none air flow should reach the outer surfaces. Furthermore the air velocity in these surfaces would be difficult to estimate.

It follows that h_{end} will be determined using the already used correlation in equation (3.16). In the gaps between plates a correlation for turbulent flow of a fluid through a long narrow channel was used (equation 3.23). This correlation is proposed by [2] to be applied in transformers' radiators when cooled by fans. The Reynolds number is presented in equation (3.24).

$$Nu_D = \frac{h_{gap} \cdot D_h}{k_{air}} = 0.023 \cdot Re_D^{0.8} \cdot Pr^{0.33} \tag{3.23}$$

$$Re_D = \frac{\rho_{air} \cdot v_{air} \cdot D_h}{\mu_{air}} \tag{3.24}$$

Where D_h is the hydraulic diameter of the cross section between plates. This diameter is different for air entering at radiator's bottom and entering at its side, equations 3.25 and 3.26. But since the plate width (W) and length (L) are much bigger than the plate spacing (S), the hydraulic diameter can be approximated to two times the plate spacing.

$$D_h = \frac{4 \cdot W \cdot S}{2 \cdot W + 2 \cdot S} \approx 2 \cdot S \tag{3.25}$$

$$D_h = \frac{4 \cdot L \cdot S}{2 \cdot L + 2 \cdot S} \approx 2 \cdot S \tag{3.26}$$

To calculate the air flow rate, the nominal flow rates of the fans cooling the radiator are summed and divided by the number of existing gaps ($N - 1$). Then the air velocity is calculated dividing this air flow by the cross area. Equations 3.27 and 3.28 were used for bottom and side ventilation, respectively.

$$v_{air} = \sum Q_{fan} / (N - 1) / (W \cdot S) \tag{3.27}$$

$$v_{air} = \sum Q_{fan} / (N - 1) / (L \cdot S) \tag{3.28}$$

For the air forced convection between plates, properties were evaluated at air average temperature. This temperature was also used to calculate the cooling capacity, instead of using the room temperature. This implies arbitrating air outlet temperature and then correcting it with equation 3.29.

$$P_{radiator} = \rho_{air} \cdot Q_{air} \cdot c_{p_{air}} \cdot (T_{air;out} - T_{air;in}) \tag{3.29}$$

3.2.4. Radiation

The radiation is a heat transfer mode that may assume an important role in the radiators cooling capacity. In order to include this process between the plate surface and the air a new circuit of thermal resistances must be considered, as shown in Figure 27.

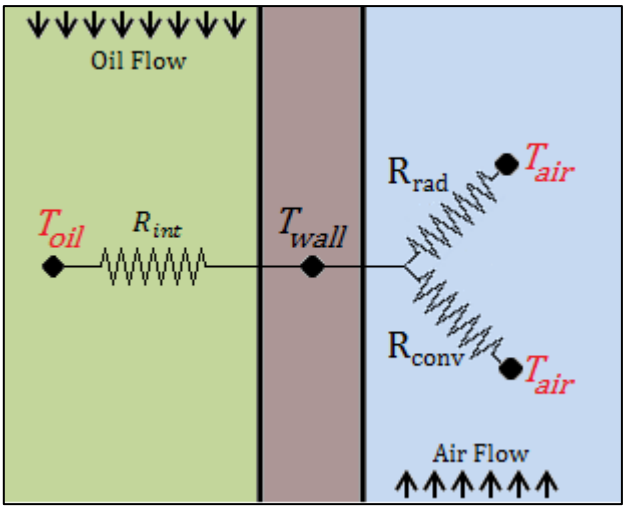

Figure 27 – Thermal resistances circuit considering radiation.

Having one resistance in series with other two in parallel, the equivalent is calculated using (3.30).

$$R_{global} = R_{int} + \frac{1}{\frac{1}{R_{rad}} + \frac{1}{R_{conv}}} \tag{3.30}$$

Where R_{rad} and R_{conv} are thermal resistances of radiation and air convection, respectively. The air convection resistance was calculated in the same way as stated previously.

A large percentage of the radiation emitted by the inner plates' surfaces will be absorbed by the opposite ones. The view factor concept was used to account the radiation that doesn't hit the other plates.

According to [17], the view factor for two aligned parallel rectangles can be estimated using equation 3.31.

$$F = \frac{2}{\pi \cdot x \cdot y} \cdot \left[\ln \left[\left(\frac{(1+x^2)\cdot(1+y^2)}{1+x^2+y^2} \right)^{\frac{1}{2}} \right] + x \cdot (1+y^2)^{\frac{1}{2}} \cdot \tan^{-1}\left(\frac{x}{(1+y^2)^{\frac{1}{2}}} \right) + y \cdot (1+x^2)^{\frac{1}{2}} \cdot \tan^{-1}\left(\frac{y}{(1+x^2)^{\frac{1}{2}}} \right) - x \cdot \tan^{-1} x - y \cdot \tan^{-1} y \right] \tag{3.31}$$

Where F is the view factor and represents the fraction of radiation that leaves one surface and reaches the other. The parameters x and y are calculated with 3.32 and 3.33.

$$x = \frac{L}{S} \tag{3.32}$$

$$y = \frac{W}{S} \tag{3.33}$$

To calculate the radiation dissipated by the plates and corresponding thermal resistances, equations 3.34 to 3.37 were used.

$$P_{rad;gap} = (F-1) \cdot \varepsilon \cdot \sigma \cdot A_{ext} \cdot (T_w^4 - T_{air}^4) \tag{3.34}$$

$$P_{rad;ends} = \varepsilon \cdot \sigma \cdot A_{ext} \cdot (T_w^4 - T_{air}^4) \tag{3.35}$$

$$R_{rad;gap} = \frac{T_w - T_{air}}{P_{rad;gap}} \tag{3.36}$$

$$R_{rad;ends} = \frac{T_w - T_{air}}{P_{rad;gap}} \tag{3.37}$$

Where ε is the surface emissivity and σ is the Stefan–Boltzmann constant ($5.67 \cdot 10^{-8}\ Wm^{-2}K^{-4}$).

3.3. CFD Simulations Methodology – AF

In order to evaluate the radiator behaviour in ONAF and ODAF cooling states, CFD simulations were performed in *Ansys Fluent v.15*. The objectives of the conducted simulations were:

- Evaluate the entry region for different plate lengths and its impact on the cooling capacity;
- Estimate the radiators cooling capacity and compare it with the literature correlation prediction;
- Compare the surface constant temperature condition with a linear temperature profile;
- Compare cooling capacities between the two fans positions: side and bottom.

The air convection was the focus of the simulation because it represents the major heat transfer resistance, its behaviour is harder to predict with correlations and the air flow is difficult to measure in experiments. In this sequence the oil flow was not modelled being the walls' temperature an input condition.

The modelled geometry consists in a rectangular prism that represents the air gap between two radiator plates. This geometry does not reflect the real wavy shape of the plates, but modelling flat plates allows the construction of a mesh with orthogonal and fewer elements, reducing the convergence time and ensuring accuracy.

Figure 28 shows a model for plates with 2200mm length and bottom ventilation.

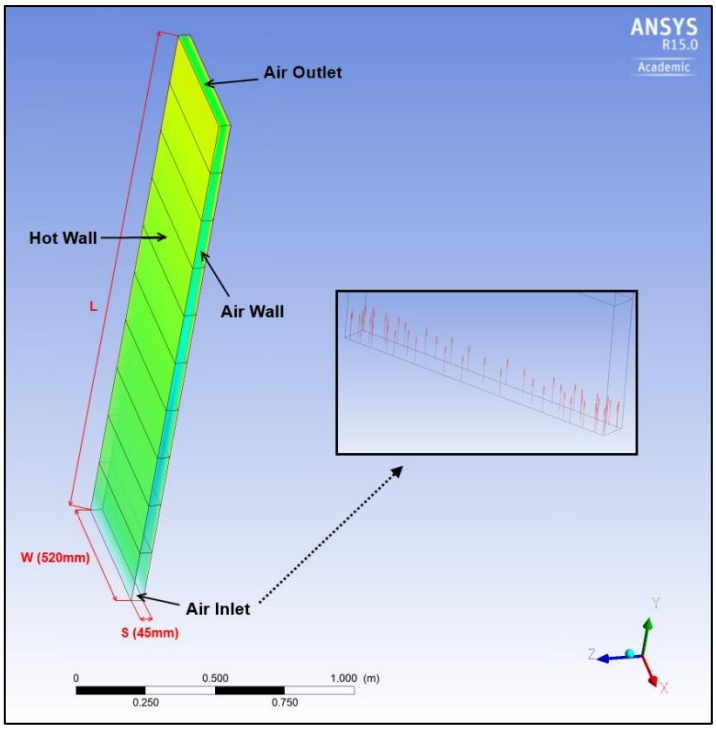

Figure 28 – Model to simulate bottom ventilation between two plates – adapted from Ansys CFD-Post.

The air walls, as named in Figure 28, are virtual walls defined with adiabatic and no slip boundary conditions. These walls were used to close the CFD model and doesn´t exist in reality. They were created to simplify the model and since *W*/*S* >10 this simplification shouldn't have a great influence on the velocity profiles. However, considering other type of boundaries may allow the evaluation of the air flow that enters or leaves the gaps from the sides.

For the side ventilation cases, the air walls change their places with the inlet at outlet surfaces. For all cases the model was divided in ten volumes in the air flow direction in order to extract local values. The boundary conditions for the different surfaces can be seen in Table 6.

Table 6 – Boundary conditions in CFD simulations

Surface Type	Boundary Conditions
Inlet	-Velocity Inlet -Constant Temperature
Outlet	-Pressure Outlet
Hot Wall	-Wall -No Slip -Temperature Linear Profile (or constant temperature)
Air Wall	-Wall -No slip -Adiabatic

Before performing the simulations, the Reynolds number was estimated using different values from fans catalogues and the obtained results were all superior to 10^4. This indicates that the air flow is in the turbulence regime and so the Standard k-ε

model with enhanced wall treatment was set. Energy equation was turned on, all residuals were set to 10^{-6} and second order solutions were set to all equations.

A mesh study was conducted in order to find an optimal grid refinement. Special attention was taken to the size of the elements next to the hot walls so that $y^+ \approx 1$. This condition is required to obtain accurate results from the enhanced wall treatment function.

The mesh was evaluated using a geometry with 800mm length (y direction), 520mm width (x direction) and 45mm in the other direction (plate spacing – z direction). The element size was established as 10% of the smaller edge, i.e. 4.5 mm, and then refinement was made in z direction. This refinement was made decreasing the element size and/or increasing the bias factor (ratio between the bigger and the smaller elements). Table 7 shows the elements size and bias factors tested in the z direction, along with the evaluation parameters used.

Table 7 – Mesh study results – refinement in z direction

	Average Element Size [mm]	Bias Factor	y+	Heat Flux [W]	Inlet Static Pressure [Pa]	Maximum Aspect Ratio	Total Number of Elements
Mesh 1	4.5	1	36.8	334.5	3.63	1.74	208800
Mesh 2	2.25	1	18.0	326.2	3.74	2.97	417600
Mesh 3	2.25	10	4.46	340.8	4.14	11.5	417600
Mesh 4	2.25	20	2.58	323.6	3.93	19.1	417600
Mesh 5	1.4	30	1.26	316.5	3.85	38.6	689040
Mesh 6	1.4	35	1.12	316.3	3.85	43.3	689040
Mesh 7	1.3	40	0.95	316.2	3.84	50.8	730800

Also velocity profiles were analysed to ensure their independence from the grid. These profiles were taken in middle lines in the geometry, indicated in Figure 29, and the results for different meshes are shown in from Figure 30 to Figure 32.

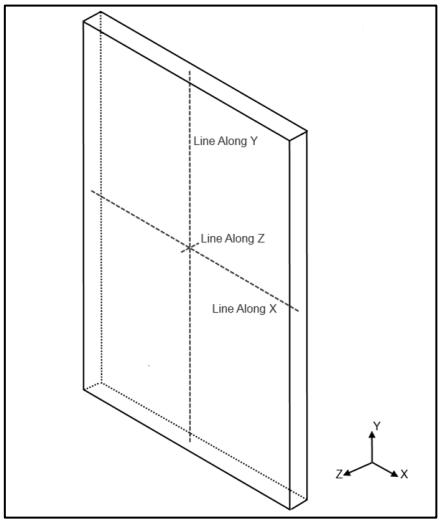

Figure 29 – Middle lines where velocity profiles were analysed.

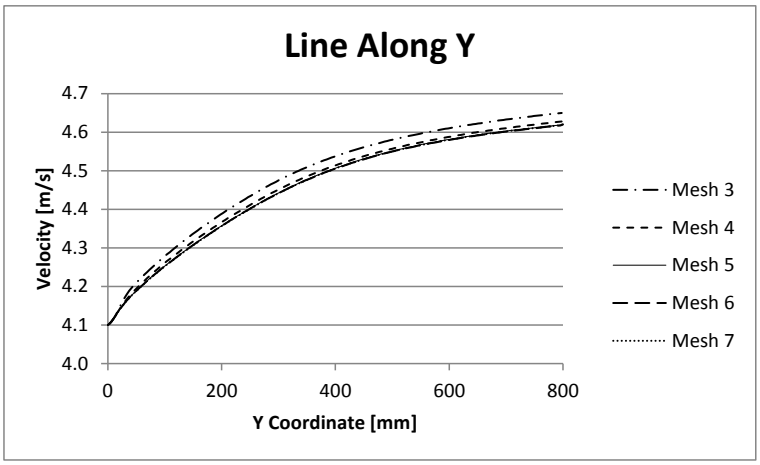

Figure 30 – Velocity profile in the middle line along Y coordinate.

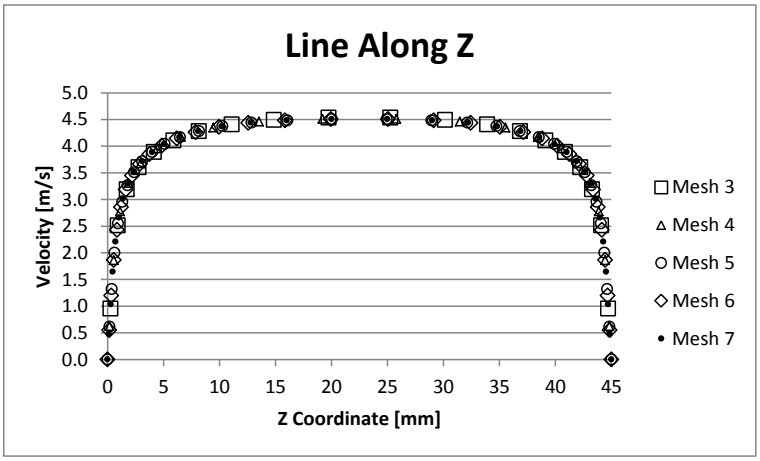

Figure 31 - Velocity profile in the middle line along Z coordinate.

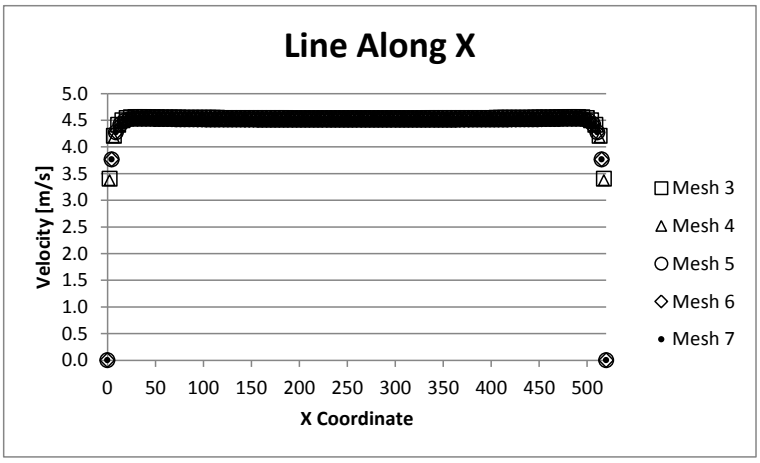

Figure 32 - Velocity profile in the middle line along X coordinate.

Analysing the above results and Table 7, it can be seen that the heat flux, the inlet static pressure and the velocity profile along Y coordinate are stabilized at mesh 5. The other two velocity profiles are similar to all meshes. Regarding y^+ condition, it is only verified at meshes 6 and 7. This grid refinement carries an increase in the number and the maximum aspect ratio of elements, but they remain structured hexahedral elements. In order to ensure accuracy in the results, mesh 7 was selected to conduct the CFD simulations. This mesh can be seen in Figure 33.

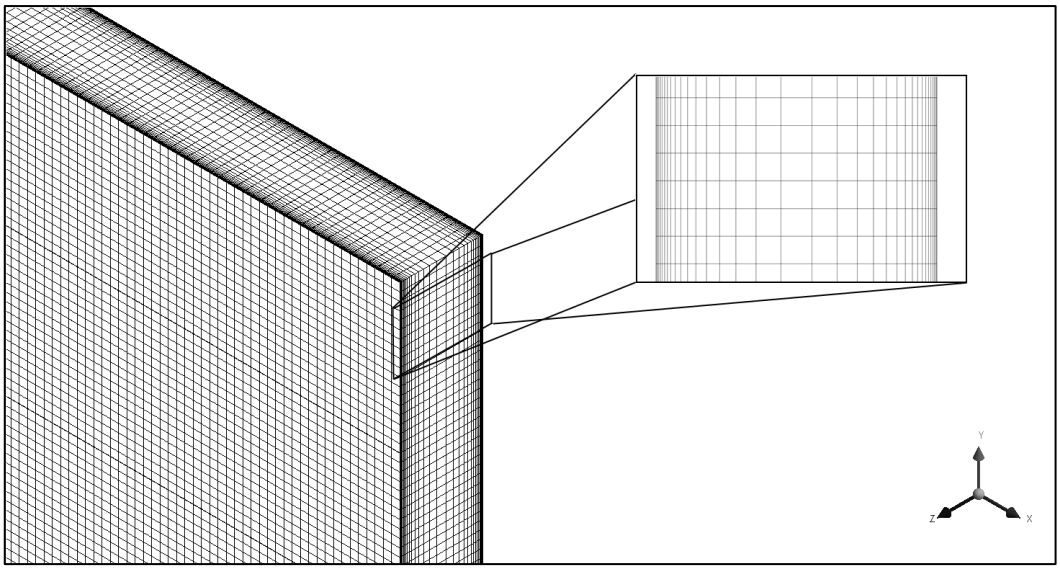

Figure 33 - Mesh 7 corner view and zoom at the side.

A base case was established with the conditions indicated in the second column of Table 8. The parameters were changed (values in Table 8) creating different combinations and a total of 56 simulations were performed with and average elapsed time of 32 minutes per simulation.

Table 8 – Parameters values for different simulations

	Base Case Value	Other Values
Hot Walls Top Temperature [ºC]	50.9	43.9 63.8 75.8
Hot Walls Temperature Drop [ºC]	14.1	0 7.1 21.2
Plate Length [mm]	2200	800 1000 1500 3300
Air Inlet Temperature [ºC]	25.8	0 40
Air Inlet Velocity [m/s]	4.10	(Values in Annex B)
Plates in Series* [-]	1	2, 4 and 6

*This parameter is only applicable to side ventilation.

In a transformer, radiators are typically disposed in groups. For side ventilation, one group of fans is responsible for cooling one group of radiators. In these cases air flow will travel a distance equal to the plate width times the number of radiators in the group. Geometries with different widths were created to simulate these situations, representing two, four and six plates in series (last parameter in Table 8).

3.4. Experimental Details – AN

Experimental work was carried out to evaluate the cooling capacity of radiators at ODAN state. The experimental apparatus was provided by Efacec and included a radiator with seven plates of 800mm. This radiator was connected to an acrylic tank with a transformer coil in a one third scale, where the oil was heated before entering at the radiator's top. After cooling in the radiator the oil returned to the tank driven by a pump. The oil flow rate was measured with an ultrasonic flow meter and its temperature was measured at radiator's inlet and outlet using temperature sensors. The equipment described can be seen in Figure 34.

Figure 34 – Experimental equipment used.

Two experiments were performed at the oil flow rate of 0.48 m^3/h with different radiator inlet temperatures of 36ºC and 58ºC. The cooling capacity was estimated using equations 3.38 and 3.39.

$$P_{radiator} = \dot{m}_{oil} \cdot c_{p_{oil}} \cdot (T_{oil;in} - T_{oil;out}) \tag{3.38}$$

$$\dot{m}_{oil} = \rho_{oil} \cdot Q_{oil} \tag{3.39}$$

The oil properties (ρ_{oil} and $c_{p_{oil}}$) where determined using equations from Annex A. The inlet and outlet temperatures during the experiments are presented in Figure 35 and in Figure 36, for the first and second experiments respectively.

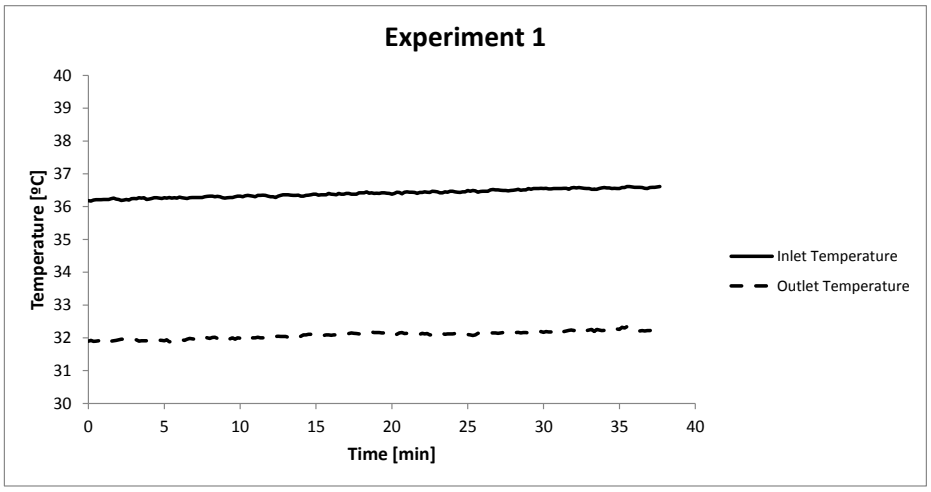

Figure 35 – Inlet and outlet temperature during experiment 1.

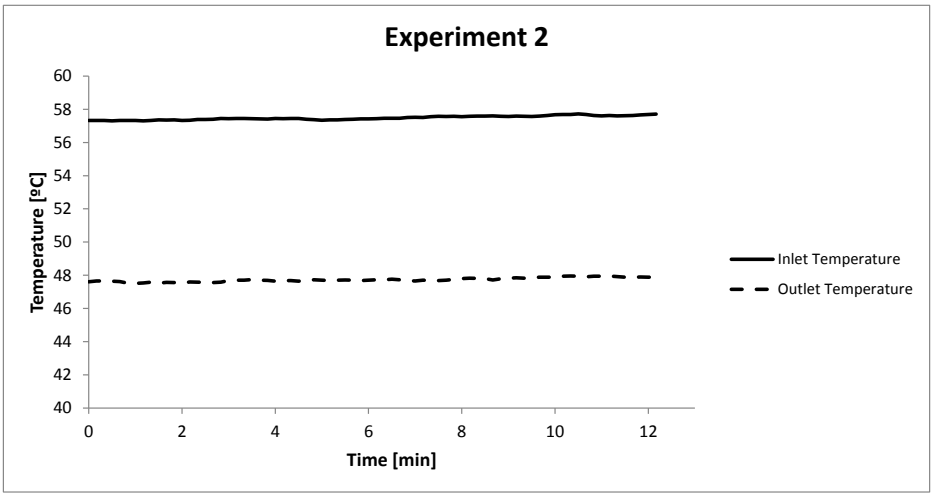

Figure 36 - Inlet and outlet temperature during experiment 2.

For the first experiment 227 values of both temperatures were recorded by an automaton and 18 values of oil flow rate were registered manually. Likewise, for the second experiment 74 values for temperatures were registered and 11 for the oil flow rate.

An uncertainty analysis was conducted for the two experiments. The registered values were processed statistically to estimate the random uncertainty and information from the equipment's catalogues was used to evaluate systematic uncertainty. The total uncertainty of each variable ($T_{oil;in}$, $T_{oil;out}$ and Q_{oil}) was obtained with equation 3.40.

$$U_x = \sqrt{P_x^2 + B_x^2} \tag{3.40}$$

Where U_x , P_x and B_x are the total, random and systematic uncertainties, respectively. Using the software *EES* (*Engineering Equation Solver*), the uncertainty propagation was calculated and consequently the total uncertainty for the cooling capacity was obtained with a confidence interval of 95%.

The procedure of uncertainty analysis is described in Annex C.

4. Results and Discussion

In this chapter the results are presented in two sections: Air Forced Convection and Air Natural Convection. The results from calculation methodologies are compared with other sources (CFD, experiments and transformers' operational tests).

4.1. Air Forced Convection

The CFD simulations are the central focus of this section. In the first part, the cooling capacities for flat plates in different conditions are presented, obtained directly from CFD simulations. These results are compared with the calculated results using the literature correlations presented previously. Then new correlations are formulated with the CFD data, followed by a comparison between side and bottom ventilations. In the last part, one of the new correlations is introduced in the calculation methodology and it is applied in a real transformer case. In this case, the results using literature and using the new correlation are compared with operational tests performed by the company.

4.1.1. CFD Simulation Results

The calculation procedure for air forced convection, previously presented on subsection 3.2.3., was applied to flat plate geometry in order to allow the direct comparison with CFD simulation results.

The cooling capacities are evaluated varying parameters one or two at the time, whereas the other parameters are kept constant at the base case values. These values are presented in Table 9.

Table 9 – Base case parameters values

Base Case Values				
Hot Walls Top Temperature	Hot Walls Temperature Drop	Plate Length	Air Inlet Temperature	Air Inlet Velocity
50.9 ºC	14.1 ºC	2200 mm	25.8 ºC	4.1 m/s

Figure 37 shows, for bottom ventilation, the cooling capacity variation with the plates' length. The respective data is showed in Table 10.

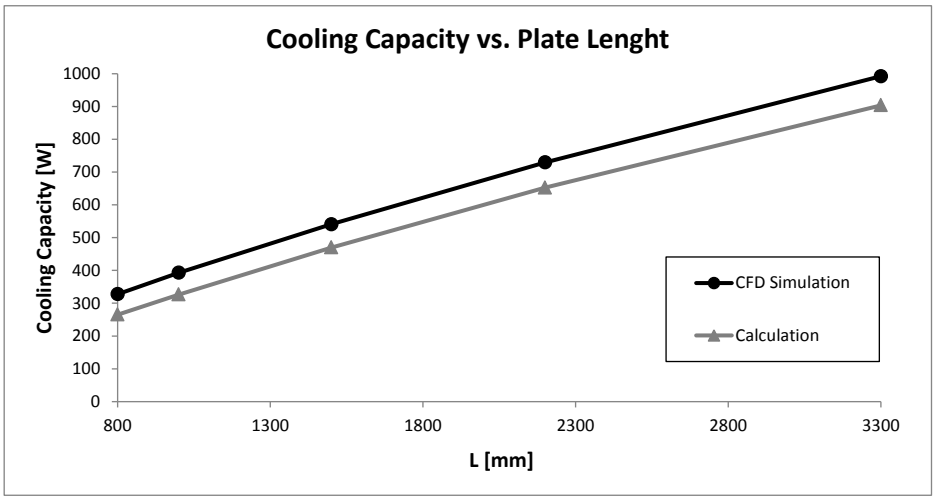

Figure 37 – Variation of cooling capacity with plate length; bottom ventilation.

Table 10 – Cooling capacities for different plate lengths and deviations of calculus from CFD results

Cooling Capacity [W]	**L[mm]**				
	800	1000	1500	2200	3300
CFD Simulation	327.7	392.8	540.7	729.2	992.0
Calculation	265.0	326.2	469.6	652.2	903.5
Deviation [%]	19.1%	17.0%	13.2%	10.6%	8.9%

It can be seen in the results that the cooling capacities predicted from the calculation procedure is always below the values provided by CFD simulation. The percentage deviation decreases with the plate length, indicating that the air flow isn't fully developed in all cases and entrance effects should be taken into account since the heat transfer is enhanced in the entry region. The evolution of both curves presented in Figure 37 also shows that the variation is not linear, which indicates that the heat transfer is not proportional to the plates' area. This can be justified also with the entry region effect: for longer plates a greater portion of the flow is fully developed having a lower average heat transfer rate. Figure 38 presents the temperature distribution, for different plates' length, in a vertical section at the middle of the plates' width.

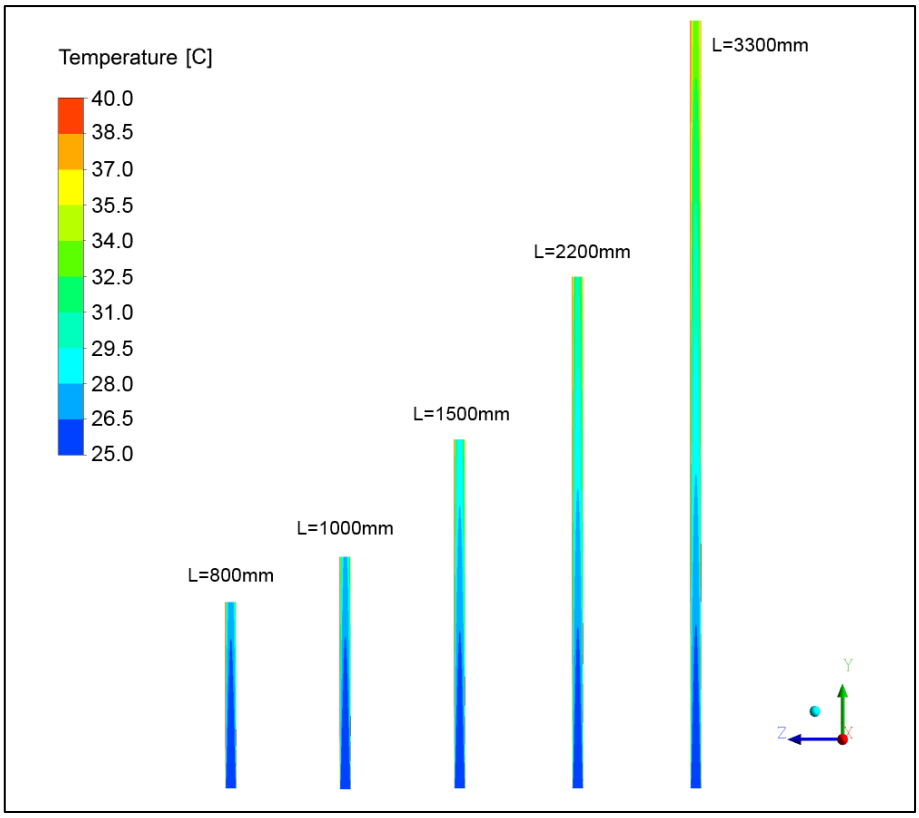

Figure 38 – CFD temperature distribution between plates in a vertical section at the middle of the plates' width.

The cooling capacities for different top wall temperatures are plotted in Figure 39, and the respective data is shown in Table 11. The impact of varying the wall temperature drop is presented for two plate lengths, 2200 and 3300mm, on left and right sides of Figure 40, respectively. The numerical values can be seen in Table 12 and Table 13.

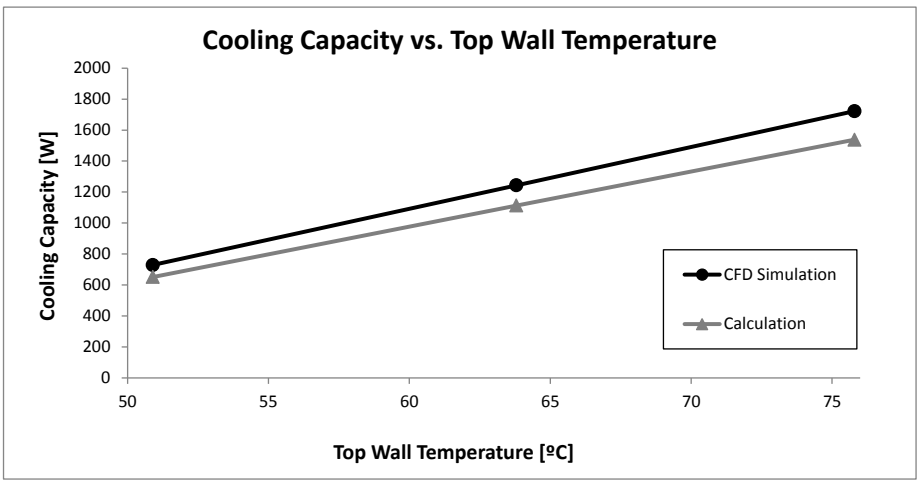

Figure 39 - Variation of cooling capacity with top wall temperature; bottom ventilation.

Table 11 - Cooling capacities for different top wall temperatures and deviation of calculus from CFD results

Cooling Capacity [W]	Top Wall Temperature [ºC]		
	50.9	63.8	75.8
CFD Simulation	729.2	1243.8	1722.7
Calculation	652.2	1113.4	1538.2
Deviation [%]	10.6%	10.5%	10.7%

Looking at Table 11, the percentage deviation remains practically the same revealing that the calculation procedure follows the simulations' pattern for different top wall temperatures.

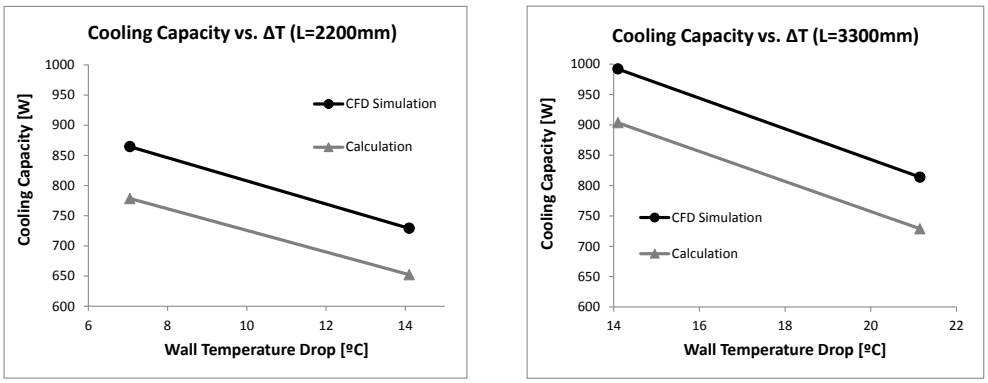

Figure 40 - Variation of cooling capacity with wall temperature drop; bottom ventilation.

Table 12 - Cooling capacities for different wall temperature drops, with L=2200mm.

Cooling Capacity [W] (L=2200mm)	ΔT on wall [ºC]	
	7.1	14.1
CFD Simulation	864.5	729.2
Calculation	778.4	652.2
Deviation [%]	10.0%	10.6%

Table 13 - Cooling capacities for different wall temperature drops, with L=3300mm.

Cooling Capacity [W] (L=3300mm)	ΔT on wall [ºC]	
	14.1	21.2
CFD Simulation	992.0	813.8
Calculation	903.5	728.7
Deviation [%]	8.9%	10.5%

The above results show that for greater temperature drops the cooling capacity is lower. Since top temperature is maintained constant, greater temperature drops imply lower bottom wall temperatures and consequently a lower average temperature. This explains why the cooling capacity decreases. On the other hand, having a lower average wall temperature shouldn't influence much the deviation between calculations and CFD

results since this parameter has been altered also in a previous case (the one from Table 11) and it didn't influence the deviations. However, as the temperature drop increases the case gets more different from the constant surface temperature condition, which is an assumption in the literature correlation. This explains the deviation increase.

Since literature correlations used in the calculation procedures were created for surfaces with constant temperature, a certain error is present when using them at the radiators case (non-constant linear temperature profile). To evaluate this error, one simulation was conducted with constant wall temperature at the average value between top and bottom temperatures of the base case. The results were compared with the ones from the base case (with temperature profile on wall) and from calculation procedure; this comparison can be seen in Figure 41 and Table 14.

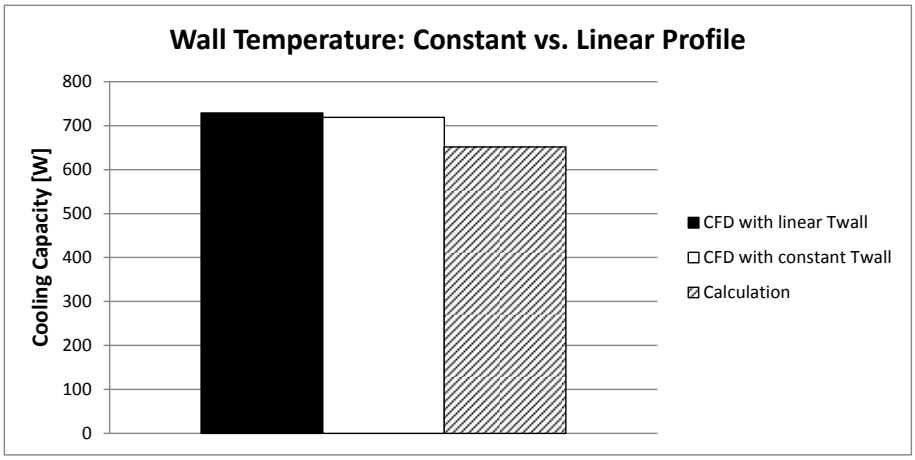

Figure 41 – Comparison between linear temperature profile and constant temperature conditions.

Table 14 – Cooling capacity for linear temperature profile and constant temperature conditions.

	Cooling Capacity [W]
CFD with linear T_{wall}	729.2
CFD with constant T_{wall}	718.8
Calculation	652.2

The cooling capacity from calculation in Table 14 presents deviations of 10.5% and 9.3% from the simulation with linear temperature profile and the one with constant wall temperature, respectively. These two deviations are nearly equal and so it can be said that the error of using correlations for constant wall temperature in radiators is negligible. However, as seen in Table 13, the error increases with the temperature drop, so the use of literature correlations is not recommended for great temperature drops in the walls.

The influence of air inlet temperature on cooling capacity was also analysed and the results are presented in Figure 42 and Table 15.

Cooling Capacity vs. Air Inlet Temperature

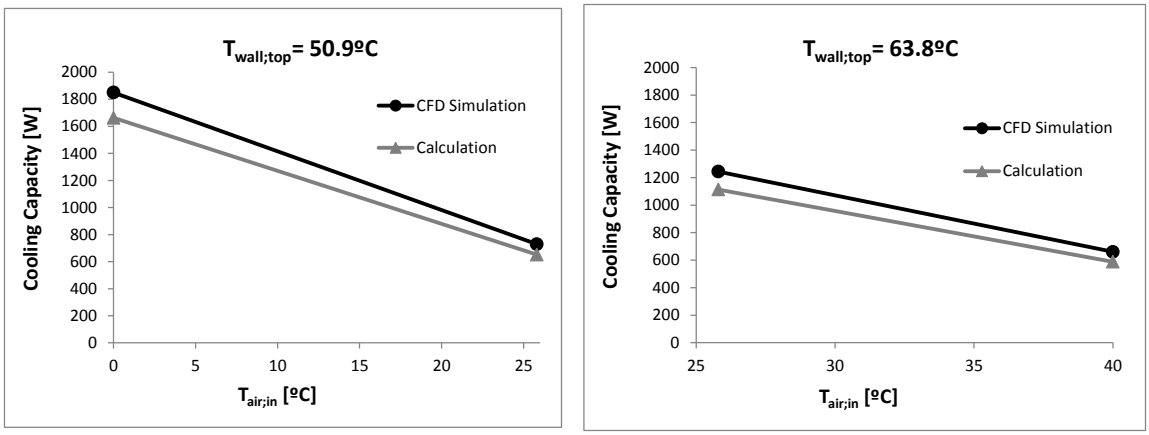

Figure 42 – Air inlet temperature influence on cooling capacity.

Table 15 – Cooling Capacities for different air inlet and top wall temperatures

	$T_{wall;top}$	50.9 ºC		63.8 ºC	
	$T_{air;in}$	0 ºC	25.8 ºC	25.8 ºC	40 ºC
Cooling Capacity [W]	CFD Simulation	1849.6	729.2	1243.8	660.1
	Calculation	1662.1	652.2	1113.4	588.3
	Deviation [%]	10.1%	10.6%	10.5%	10.9%

Evaluation of cooling capacity for air inlet temperature at 40ºC was performed with 63.8ºC in the top wall because the base case has a bottom temperature of 36.8ºC, which is inferior to 40ºC and it would lead to an unrealistic simulation (since the walls temperatures cannot fall behind the air inlet temperature). To better analyse the impact of changing air inlet temperature, the information was organized also in terms of the difference between average wall temperature and air inlet temperature ($T_{wall;ave}$ - $T_{air;in}$). This new analysis is presented in Figure 43.

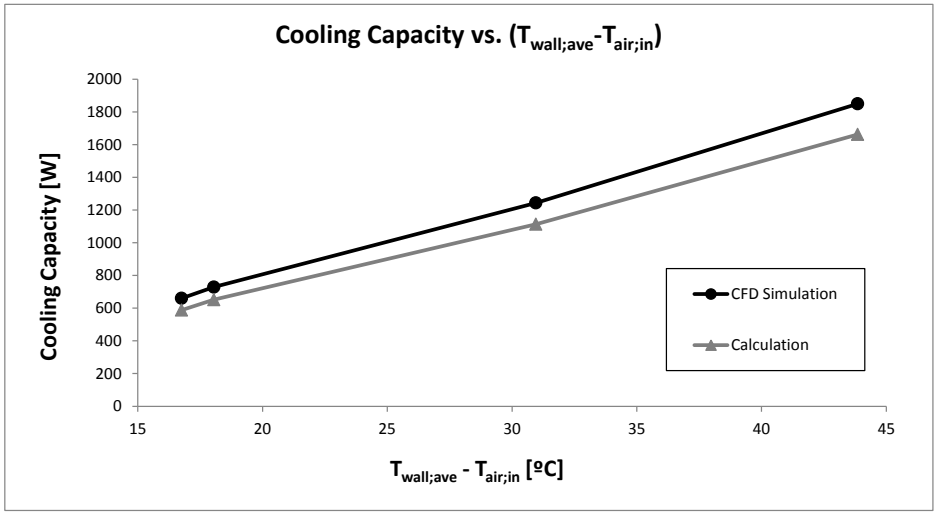

Figure 43 – Cooling capacity variation with the temperature difference between wall and inlet air.

Looking at the results it is clear that the wall and air inlet temperatures have both great influence on cooling capacity but their effect should be analysed together. For

example supposing a case with wall top at 63.8ºC and air at 40ºC, changing these values to 50.9ºC and 25.8ºC, respectively, only increases cooling capacity by 10%. This happens because although air and wall temperatures have changed a lot, the temperature difference increased only 1.3ºC. The calculation procedure follows the simulation curve along these temperature variations since the deviations in Table 15 are very similar.

For analysing air inlet velocity, 14 levels of velocities were simulated for different geometries. In Table 16 is the nomenclature attributed to different geometries in order to facilitate the comparison.

Table 16 – Nomenclature attributed to different geometries

Name	Description
2200 B	L=2200mm; Bottom Ventilation
2200 S1	L=2200mm; Side Ventilation; 1 pair of plates (W=520mm)
800 B	L=800mm; Bottom Ventilation
800 S1	L=800mm; Side Ventilation; 1 pair of plates (W=520mm)
800 S2	L=800mm; Side Ventilation; 2 pairs of plates (W=1040mm)
800 S4	L=800mm; Side Ventilation; 4 pairs of plates (W=2080mm)
800 S6	L=800mm; Side Ventilation; 6 pairs of plates (W=3120mm)

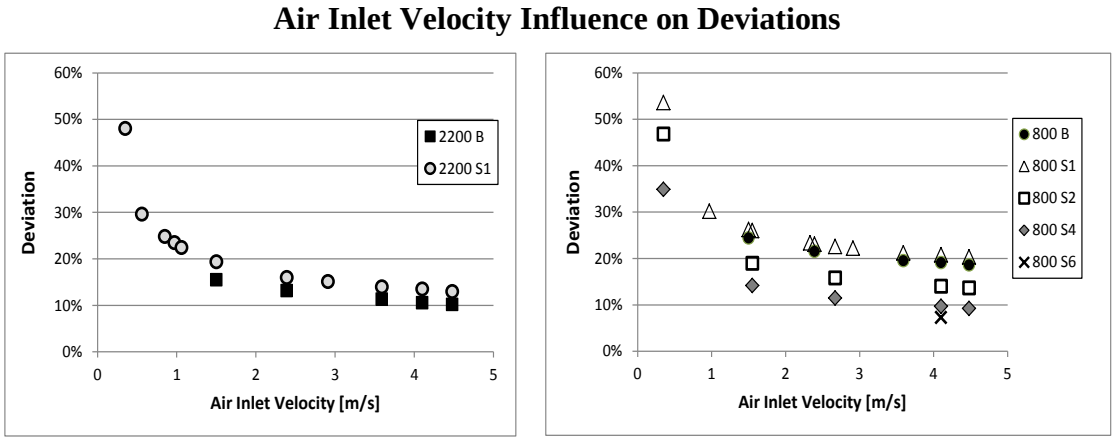

Figure 44- Deviations on cooling capacities between calculation procedures and CFD simulations, for different air inlet velocities and different geometries.

Figure 44 shows the air inlet velocity influence on deviation between calculation and simulation results, for different geometries and for side and bottom ventilation.

The results show that for all models the deviation decreases with air inlet velocity. Since the velocity profile is uniform at the entrance, higher inlet velocities imply higher air volumetric flows (and mass flows also because the inlet temperature is the same). The air temperature increase along the flow path is bigger for lower mass flows and so it can be said that for low inlet velocities greater temperature increases take place. Figure 45 shows this effect on 2200 B cases, representing for different velocities the temperature evolution in a central axis along the flow direction.

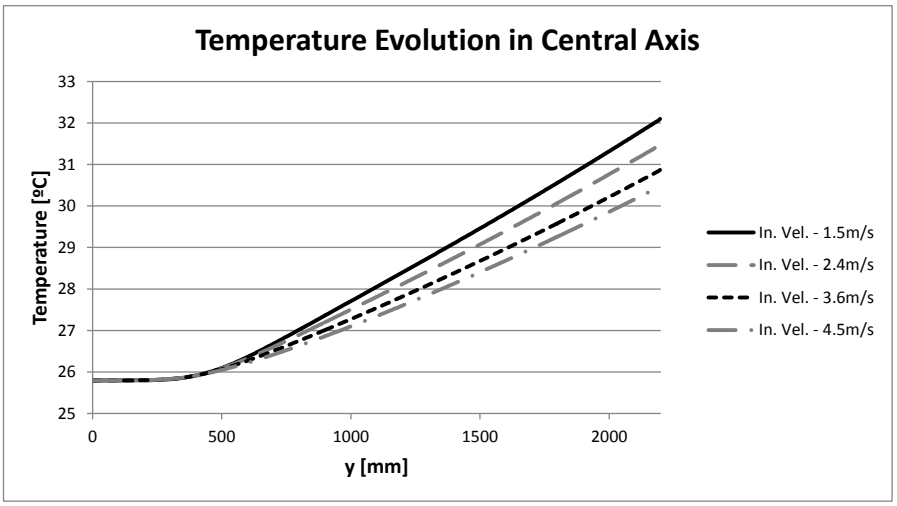

Figure 45 – Temperature evolution along flow direction for different inlet velocities.

If for smaller velocities the air temperature increases more, the density also decreases more and the velocity profile will suffer more changes. This phenomenon may be the cause for greater deviations at smaller velocities, since the correlations may not respond to these changes.

Is important to notice that the higher deviations occur in the cases with velocities below 2 m/s, where the Reynolds number is always above the turbulence lower limit. Since calculation procedures were performed considering turbulent correlations and simulations were conducted with a turbulence model, both methodologies may be inaccurate out of the turbulence region.

Still analysing Figure 44, the different deviations between models can be explained by the entry region effect. For example, the air flow travels a shorter distance in 800 S1 cases (travelled distance of 520 mm) and higher deviations take place since the entry length is a higher percentage of the total travelled distance. The lower deviation occurs in the 800 S6 case because it has the greater travelling distance (6 plates in series give a total distance of 3120mm).

4.1.2. Formulation of New Correlations

In the previous subsection it was showed by the results from simulations that the entry region has a great impact in the heat transfer between the walls and the air. Analysing the deviations between the calculation procedure and the simulation, it was concluded that the literature correlations used don't take into account the entrance effects. Taking this into account new correlations were developed to enhance the calculation procedure accuracy.

To develop these new correlations, Nusselt and Reynolds numbers were calculated using the data from CFD. From the 56 conducted simulations, only one was excluded from this analysis because it didn't correspond to a realistic situation: the one with constant wall temperature condition. Two different correlations were developed: one for bottom and another for side ventilation.

According to [17], for turbulent internal flows a correlation of the form presented in equation 4.1 can be used to calculate the average Nusselt number considering the entry region.

$$Nu_D = Nu_{D,fd} \cdot \left[1 + \frac{C}{(x/D_h)^m}\right] \tag{4.1}$$

Where Nu_D, $Nu_{D,fd}$ and x are respectively the average Nusselt, the Nusselt in the fully developed region and the distance in the flow direction. C and m are parameters that depend on certain flow conditions, such us the nature of the inlet.

The first step was the determination of $Nu_{D,fd}$. For bottom ventilation the cases with the longer plates (3300mm) should be used to calculate $Nu_{D,fd}$ since this is the situation were the flow is most developed. However, cases with 2200 and 3300 mm plates were used as references to the fully developed flows because only 3 simulations were conducted with the longer plates and performing more simulations with this geometry would take more convergence time. Notice that in Table 10 the deviations for the 2200 and 3300mm plates are not so different (10.6% and 8.9%) which means that the assumption should cause small errors.

Figure 46 shows the Nusselt number depending on the Reynolds Number for bottom ventilation simulations. It is also presented in the figure the trend line that better fitted the values used for the fully developed condition.

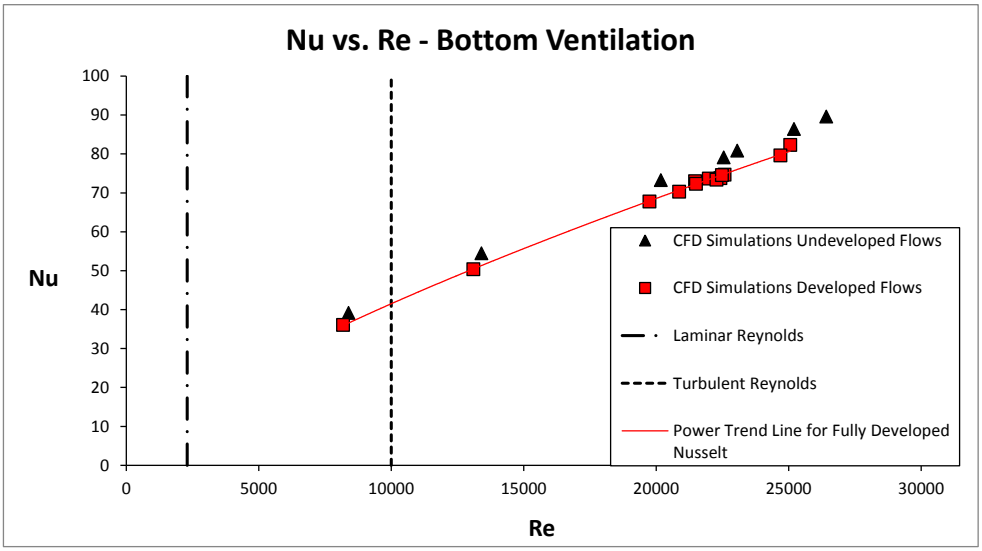

Figure 46 – Nusselt depending on Reynolds, for bottom ventilation simulations.

Table 17 – Comparison between regressions for the $Nu_{D,fd}$ for bottom ventilation

Regression Type	R^2
Exponential	0.9836
Linear	0.9975
Logarithmic	0.9845
Polynomial (order 2)	0.9978
Power	0.9987

Table 17 shows the coefficient of determination (R^2) for different types of regressions in order to know which fits better. The power function has been selected since it presents the higher R^2 and the correlation of $Nu_{D,fd}$ is presented in equation 4.2.

$$Nu_{D,fd} = 0.053 \cdot Re_D^{0.72} \tag{4.2}$$

The same procedure was performed for side ventilation and for the $Nu_{D,fd}$ were used the cases with 4 and 6 plates in series. These are the cases in which the air flow travels a greater distance, for 4 plates is 2080mm and for 6 plates is 3120mm.

When using all simulations results for side ventilation, the power regression didn't fit well to the results (as showed in Figure 47).

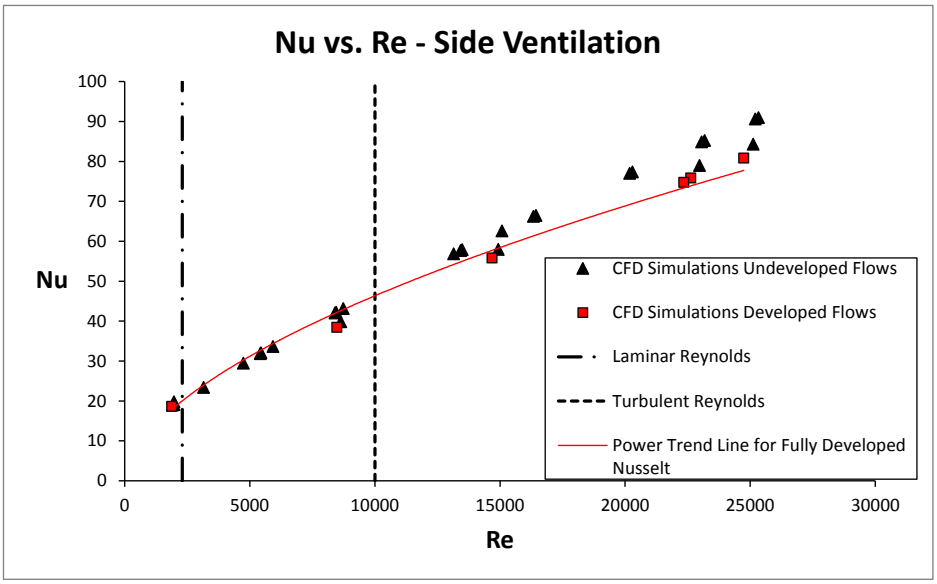

Figure 47 - Nusselt depending on Reynolds, for side ventilation simulations.

Looking at Figure 47, one can see that some points are in the laminar zone (Re<2300) and others are very close of the laminar limit. The simulations were made with a turbulence model so Nusselt values on this zone are probably overestimated – if these values were inferior the power regression would fit better. In this sequence the points in or near the laminar zone were eliminated and the results were analyzed again (Figure 48). Notice that in real radiators fans will induce velocities that correspond to the turbulent regime, so the laminar zone has not much interest to this analysis.

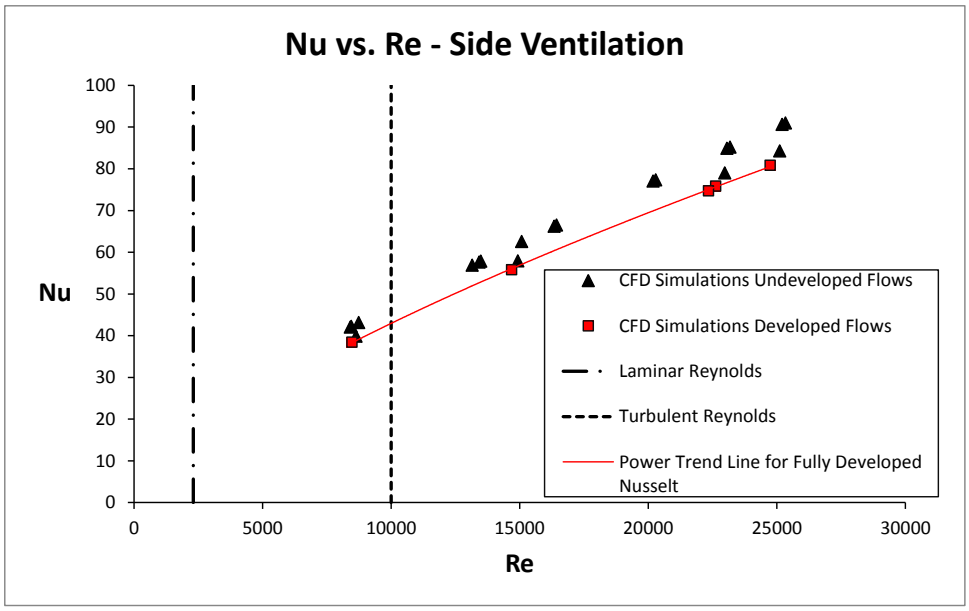

Figure 48 - Nusselt depending on Reynolds, for side ventilation simulations.

Now the power function fits well to the fully developed Nusselt. The coefficients of determination (R^2) of power, linear and second order polynomial regressions are very similar and practically equal the unit (Table 18). The power function was selected to correlate $Nu_{D,fd}$ since this is the form that is found in literature.

Table 18 - Comparison between regressions for the $Nu_{D,fd}$ for side ventilation

Regression Type	R^2
Exponential	0.9861
Linear	0.9992
Logarithmic	0.9898
Polynomial (order 2)	0.9999
Power	0.9998

The obtained correlation for side ventilation in the fully developed region is presented in equation 4.3.

$$Nu_{D,fd} = 0.072 \cdot Re_D^{0.69} \tag{4.3}$$

Both bottom and side ventilation cases were correlated with the power function for the fully developed condition, so the average Nusselt correlations will have the form:

$$Nu_D = A \cdot Re_D^B \cdot \left[1 + \frac{C}{(x/D_h)^m}\right] \tag{4.4}$$

The parameters *C* and *m* were determined by the minimization of the sum of the squared differences between simulation results and values estimated by equations 4.2 and 4.3. The results of these adjustments are shown in Figure 49 for bottom ventilation and in Figure 50 for side ventilation.

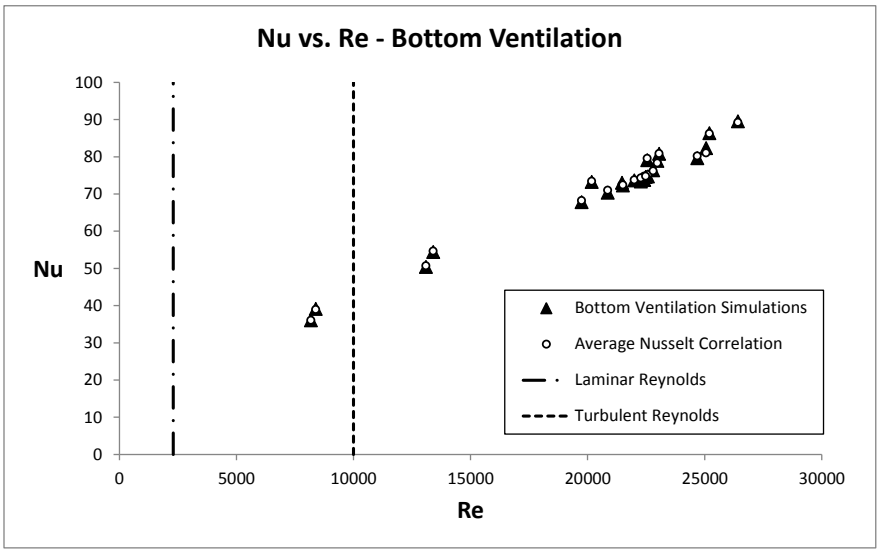

Figure 49 – Adjustment of average Nusselt correlation for bottom ventilation.

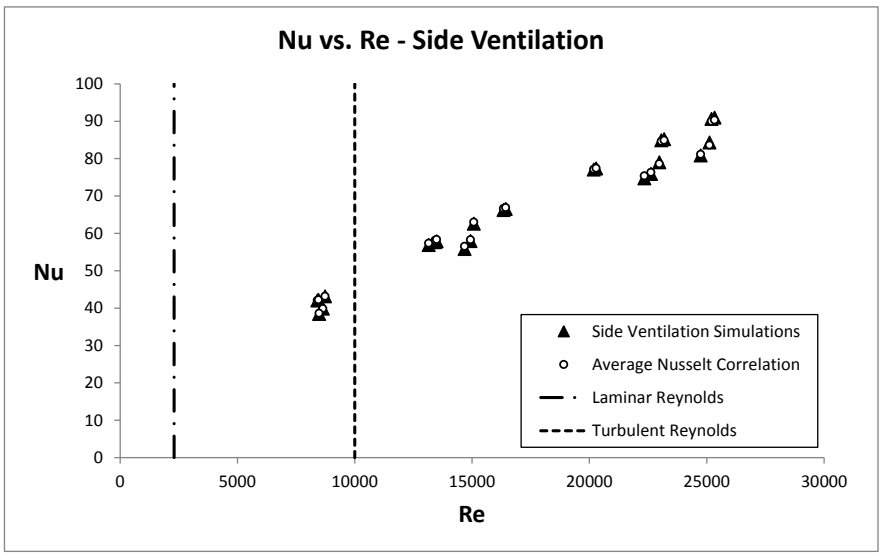

Figure 50 – Adjustment of average Nusselt correlation for side ventilation.

The final correlations have shown to adjust very well to the simulation data in both ventilation types and so the procedure to create them is concluded with success. The final correlations for bottom and side ventilations are presented in equations 4.5 and 4.6.

$$Nu_D = 0.053 \cdot Re_D^{0.72} \cdot \left[1 + \frac{52.6}{(x/D_h)^{3.1}}\right] \quad (4.5)$$

$$Nu_D = 0.072 \cdot Re_D^{0.69} \cdot \left[1 + \frac{3.16}{(x/D_h)^{2}}\right] \quad (4.6)$$

4.1.3. Bottom vs. Side Ventilation

This subsection presents a focus on the comparison between cooling the radiator plates with fans on their bottom and fans on their side. Figure 51 shows a comparison between the two cooling configurations (side and bottom) presenting cooling capacities for different air inlet velocities.

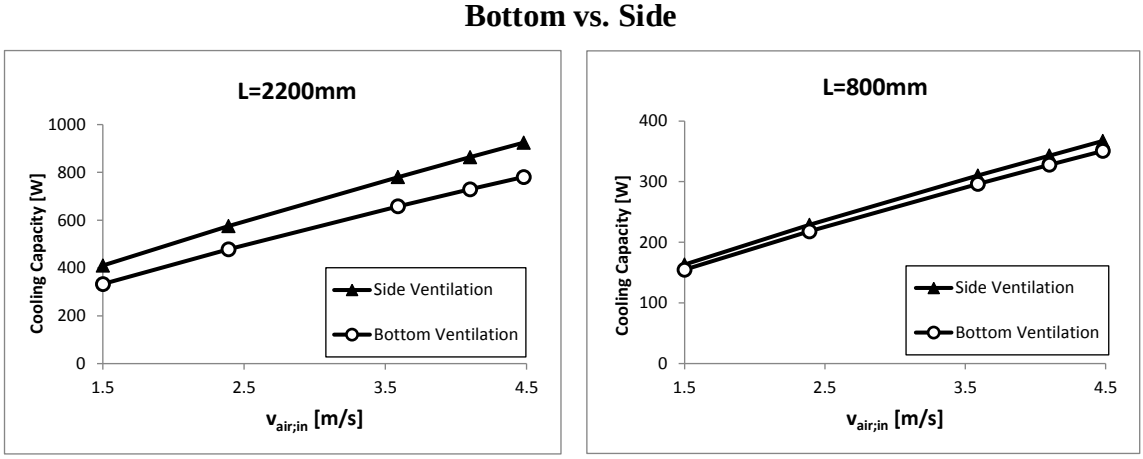

Figure 51 – Cooling capacity for different inlet velocities, comparing bottom and side ventilation; with plates of 2200mm length (left) and 800mm length (right).

In both cases (800 and 2200mm plates) the side ventilation presents higher cooling capacities for all velocities. This happens because side ventilation has larger cross section than bottom ventilation and so for the same velocity the side case has a superior air flow passing throw the plates. In the right side of Figure 51 the two curves are closer than in the left side situation because the plates' length and width are more similar, 800 and 520mm respectively, causing the cross sections and the air flows in side and bottom ventilation to more alike.

In this sequence the side and bottom ventilations were also compared introducing the same volumetric air flow rates in both cases. Figure 52 shows the cooling capacities for different air flow rates, again for 2200mm and 800mm plates.

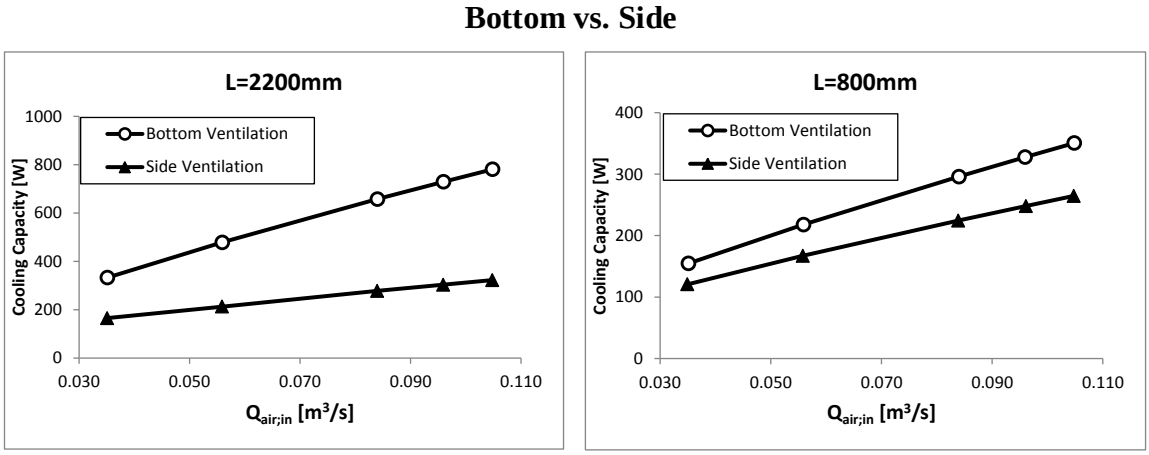

Figure 52 – Cooling capacity for different air inlet flow rates, comparing bottom and side ventilation; with plates of 2200mm length (left) and 800mm length (right).

As it can be seen in Figure 52, considering the same air flow for side and bottom cases the later one presents higher cooling capacities. Here the situation is reversed: the same air flow at the side and at bottom leads to inferior velocities in the side case since the cross section is superior. This causes lower cooling capacity for side ventilation. Notice that for the 800mm plates (right side of the figure) the curves are closer than the curves for 2200mm plates because of the same reason: side and bottom cross sections are more similar.

In the two comparisons made (fixing velocities and flow rates) one pair of plates was only considered, so it is still not known if placing pairs of plates in series makes the side ventilation more effective than bottom ventilation. To evaluate these situations, cooling capacities were estimated for multiple pairs of plates, with the same total air flow for side and bottom ventilation. A scheme for 3 pairs of plates is presented in Figure 53. The cooling capacity results are shown in Figure 54.

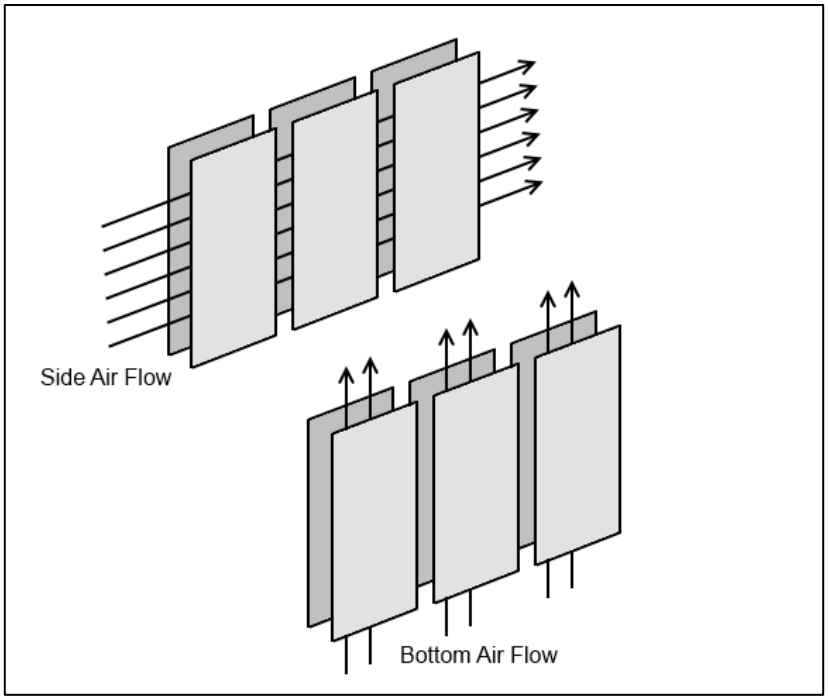

Figure 53 – Three pairs of plates cooled by side and bottom ventilation.

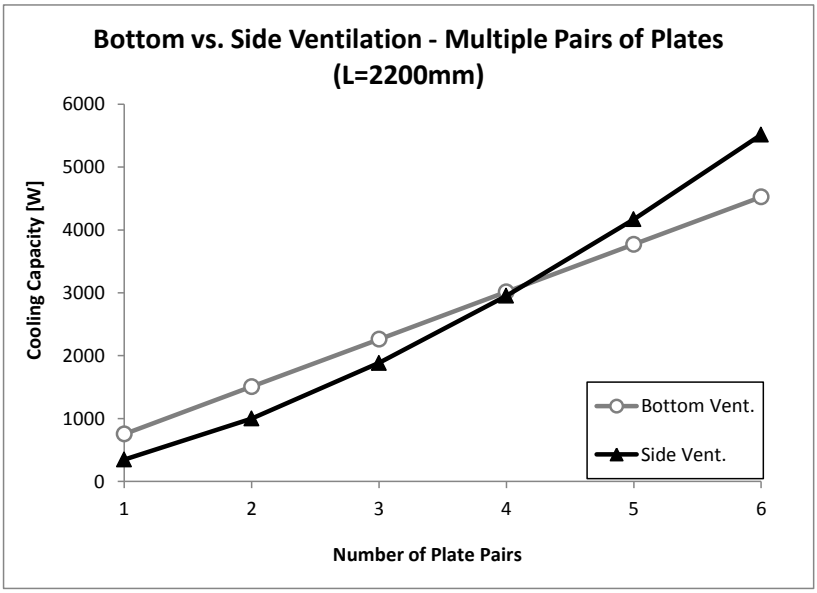

Figure 54 – Cooling capacity for different number of plate pairs; L=2200mm.

The values presented in Figure 54 were estimated with the calculation procedure but using the correlations obtained from simulation results. The analysis was performed for flat plates with 2200mm length, with the same temperature profile on the walls and air inlet temperature.

The results show that bottom ventilation is more efficient than side ventilation until 4 pairs of plates and from there forward the situation is inverted. For each pair of plates that is added to the arrangement, different things occur for the two configurations:

- For bottom ventilation the total air flow increases in the same proportion of the total cross section. Consequently the flow velocity is always the same, the average heat transfer coefficient remains unchanged and the cooling capacity increases linearly;
- For side ventilation the total air flow increases but the cross section doesn't change. Therefore the flow velocity and the average heat transfer coefficient increase, enhancing the cooling capacity and the heat transfer efficiency.

This explains the pattern of the curves in Figure 54. In fact, the situation in which side overcomes bottom ventilation is when its flow average velocity becomes superior. Following this logic, it is expected that using smaller plates the two configurations (side and bottom) equalize their average flow velocity with less pairs of plates. This was confirmed repeating the calculation for plates with 800mm length (see Figure 55).

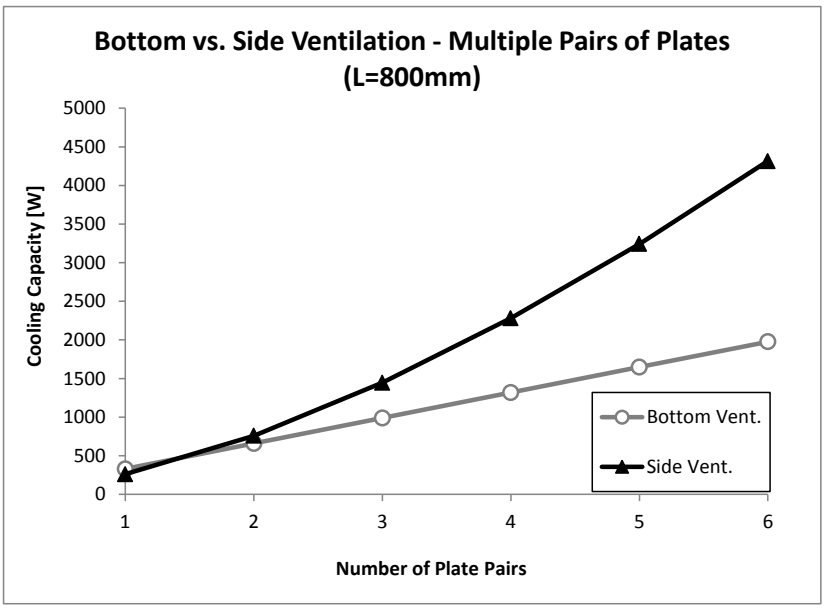

Figure 55 – Cooling capacity for different number of plate pairs; L=800mm.

Generally speaking, choosing side or bottom ventilation depends on the number of radiators in series and the length of their plates. Notice that in the studied cases it was assumed that the same quantity of air flow can be induced at the radiators side and bottom. In reality the induced air flow depends, among other things, on the number of fans cooling the radiators. Therefore another important aspect to choose side or bottom ventilation is the number of fans that can be coupled to radiators in each configuration.

4.1.4. Transformer 546A in ONAF

The calculation method was employed in a real transformer from Efacec operating in ONAF (Oil Natural Air Forced) in order to evaluate the accuracy of this methodology.

Transformer 546A is a power transformer and its cooling system consists in 12 radiators cooled by 16 fans. These components are arranged in 4 groups, having each group 3 radiators and 4 fans attached to the side of the first radiator (see Figure 56).

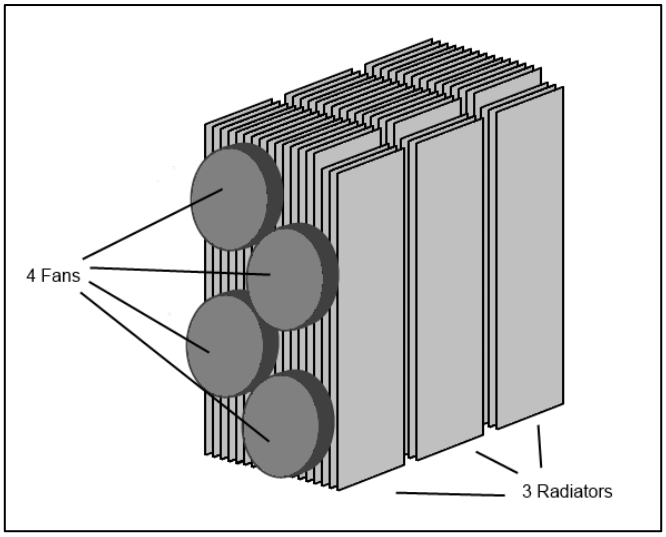

Figure 56 – Scheme of a radiator group of transformer 546A.

Each radiator has 18 plates, 15 of them with 2200mm length and the other three with 1800mm. The average cooling capacity of each radiator was estimated using values from operation tests performed on the transformer by Efacec. The test data was compared with calculation procedures with three different conditions:

- Considering the literature correlation;
- Considering the correlation obtained from simulation results for side ventilation;
- Considering the correlation obtained from simulations and adding the radiation heat transfer mode.

To make this comparison, the same values of temperature and oil flow rate reported in the test were considered in the calculation procedures. These parameters are presented in Table 19.

Table 19 - Operating conditions of transformer 546A in ONAF

Oil Flow Rate per Radiator	1.3 m^3/h
Inlet Oil Temperature	53 ºC
Room Temperature	26 ºC

The average cooling capacity per radiator is presented in Figure 57. The numerical values and the deviations from the test data are shown in Table 20.

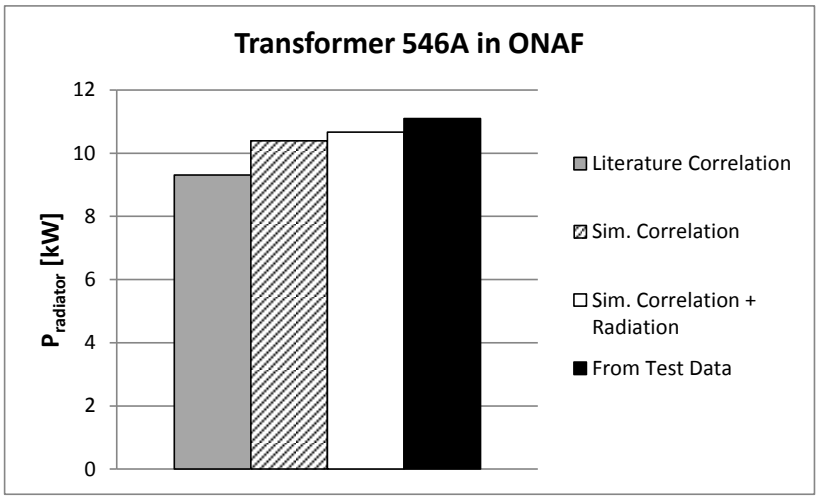

Figure 57 – Radiator's cooling capacity comparison from four different sources.

Table 20 – Radiator's Cooling Capacity and deviations from test data

	Cooling Capacity [kW]	Deviation
From Test Data	11.1	-
Sim. Correlation + Radiation	10.7	3.9%
Sim. Correlation	10.4	6.3%
Literature Correlation	9.3	16.2%

As it can be seen from the above results, the estimates provided by calculation procedures with the new correlation reveal low deviations from test results (3.9% considering radiation and 6.3% considering only air convection). The radiation approach seems adequate since it led to a result with an inferior deviation from the operation test. The literature correlation shows a higher deviation and so its application to vertical plate radiators is not recommended.

Notice that due to the nature of the performed test, the uncertainty of the cooling capacity value cannot be calculated. Making experimental tests with uncertainty analysis allow a better validation of the calculation procedure.

4.2. Air Natural Convection

The calculation procedure for air natural convection was evaluated by its application in three case studies: the experiments previously reported in section 3.4., a transformer from Efacec and the experiments conducted in [5] (already mentioned on the State of the Art).

4.2.1. Experimental Results

As stated before, two experiments were conducted on a radiator with 7 plates of 800mm length. The average values for the oil flow rate, the oil temperature at radiator's inlet and outlet, the room temperature and the calculated cooling capacity are listed in Table 21.

Table 21 – Experimental average values

	Experiment 1	Experiment 2
Room Temperature [ºC]	15.5	15.6
Inlet Oil Temperature [ºC]	36.4	57.5
Outlet Oil Temperature [ºC]	32.1	47.7
Oil Flow Rate [m^3/h]	0.48	0.47
Cooling Capacity [W]	955	2135

The total uncertainties with 95% confidence of the cooling capacity values are presented in Table 22.

Table 22 – Cooling capacity uncertainty for the two experiments

	Experiment 1	Experiment 2
Total Uncertainty	±183 W (19%)	±244 W (11%)

The above results show a high uncertainty associated to the experimental cooling capacity values (maximum of 19%). The experiments were performed at a very low oil flow rate, in which the flow meter presents lower accuracy (5% of systematic error by the manufacturer's catalogue). To obtain a systematic error of 1%, the oil flow rate should be equal or superior to 2.3 m^3/h. The temperature values present lower uncertainties (average of 1.3%) than the oil flow rate, but its contribution to the uncertainty on the cooling capacity is higher in the first experiment (according to *EES software*). So the total uncertainty on cooling capacity can be reduced operating at higher flow rates and temperatures. More details about the uncertainty analysis are presented on Annex C.

The experimental results were compared with calculation procedures making four different considerations that are described in Table 23. The results provided by these methods are presented in Table 24.

Table 23 – Nomenclature for calculation procedures according to different considerations

Name	Description
Method 1	Using the isolated vertical plate correlation for the air convection between plates. This correlation is presented in equation 3.16 (section 3.2.)
Method 2	Using the parallel plate correlation for the air convection between plates. This correlation is presented in equation 3.18 (section 3.2.)
Method 1 Rad	The same as Method 1 but including the radiation heat transfer mode.
Method 2 Rad	The same as Method 2 but including the radiation heat transfer mode.

Table 24 – Cooling capacity from calculation methods

Cooling Capacity [W]	Experiment 1	Experiment 2
Method 1	479	1125
Method 2	434	1001
Method 1 Rad	604	1380
Method 2 Rad	562	1266

The cooling capacities obtained from experiments and from calculation procedures are plotted in Figure 58. The calculation deviations from the experimental values are presented in Table 25.

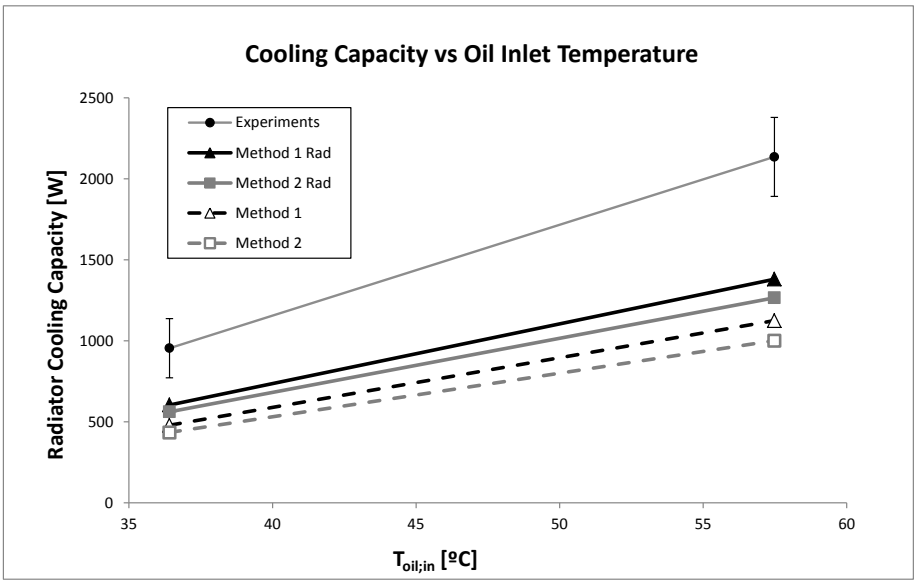

Figure 58 – Comparison between experimental and calculation cooling capacities values.

Table 25 – Deviation of calculated cooling capacities from the experimental results

Deviations	Experiment 1	Experiment 2	**Average**
Method 1 Rad	37%	35%	**36%**
Method 2 Rad	41%	41%	**41%**
Method 1	50%	47%	**49%**
Method 2	55%	53%	**54%**

The calculation procedures show high deviations (from 35% to 55%) on the cooling capacity prediction, which are out of the uncertainty range associated to the experimental results. The values obtained from calculation methodology are all below the ones provided by the experiments and it can be explained by three possible hypotheses:

- Since the plates are short the air boundary layers on the plates' surfaces remain well separated, like two vertical isolated plates but with a higher heat transfer rate. According to [20], the heat transfer in a parallel plate arrangement can be higher than in the isolated plate case, duo to induced flow by the chimney effect;

- The literature correlations are unable to reflect the heat transfer process in radiators, since the plates aren't flat and the temperature is not constant along the surfaces – two conditions imposed by the correlations;
- The radiation approach is under estimated.

The first two hypotheses can both be solved creating new correlations to the vertical plate radiators. For this proposition more experiments or simulations have to be performed. The third hypothesis is improbable to be the major cause of deviations, since the radiators plates present a symmetric disposition causing a surface to intercept a great fraction of the radiation leaving the other surface in front.

Despite of the high deviations presented by the calculation, notice that considering the radiation mode enabled a significant increase in the cooling capacity; it increased on average 24% for Method 1 and 28% for Method 2.

4.2.2. Transformer 546A in ONAN

The four calculation methods previously described in Table 23 were applied in one Efacec's transformer case. The transformer is the model 546 A, already described in subsection 4.1.4. but this time operating in the ONAN state (Oil Natural Air Natural).

The average cooling capacity of each radiator was estimated using values from operation tests performed on the transformer by the company. To compare this test with the calculation procedure the same values of temperature and oil flow rate were used and are presented in Table 26.

Table 26 – Operating conditions of transformer 546A in ONAN

Oil Flow Rate per Radiator	1.4 m^3/h
Inlet Oil Temperature	60.3 ºC
Room Temperature	23.5 ºC

The comparison between the test data and the results from calculation methods is presented in Figure 59 and Table 27.

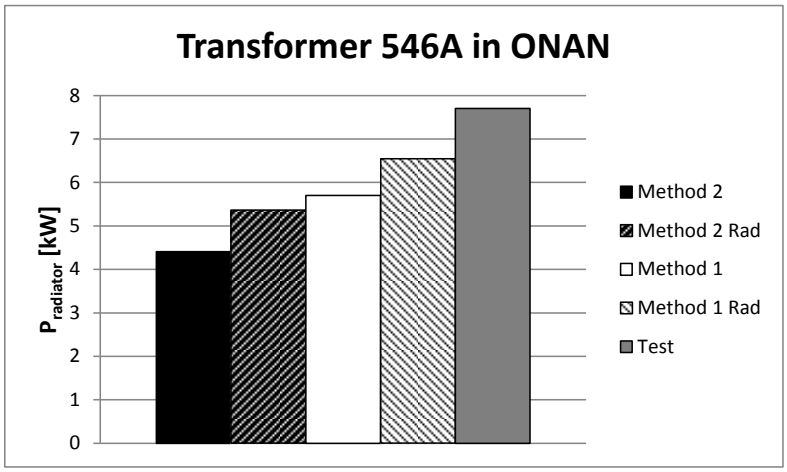

Figure 59 – Radiator's cooling capacity results.

Table 27 – Cooling capacity for one radiator of transformer 546A in ONAN

	Radiator's Cooling Capacity [kW]	Deviation from Test
Test	7.7	-
Method 1 Rad	6.5	15%
Method 1	5.7	26%
Method 2 Rad	5.4	30%
Method 2	4.4	43%

The results show once again that the cooling capacity predicted by calculations procedures is below the test results. Notice that the deviations are much lower than in the case presented in the previous subsection. Since the radiators of transformer 546A have plates of lengths 1800 and 2200mm, longer than the ones of the previous case (800mm), it is expected that a greater portion of the air flow is developed. This way the average heat transfer rate is lower for the 546A case and it explains why the calculation results are closer from the test.

Looking at the values in Table 27, it can be seen that now Method 1 gives a higher cooling capacity than Method 2 Rad, unlike in the radiator with 800mm length. This is justified by the different responses that the two correlations have in the cooling capacity by changing the length of the plates. In order to clearly see these responses, the 4 methods were compared in terms of cooling capacity variation with the plates' length. The comparison was performed considering a radiator with 18 equal plates and fixing the other parameters at the values presented in Table 26. The results can be seen in Figure 60.

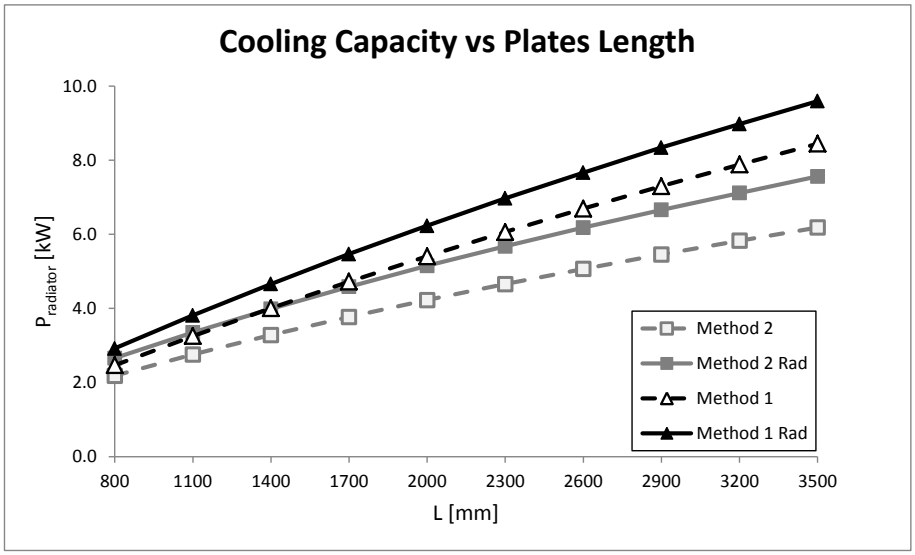

Figure 60 – Cooling capacity calculated by the four methods for different plate lengths.

In Figure 60 can be seen that the curves present different slopes and the results present larger differences for longer plates. It can be seen also that Method 1 starts to exceed Method 2 Rad at $L \approx$1400mm.

4.2.3. Hyosung Experiments

As stated before in the State of the Art section, Min-gu Kim et al. [5] performed experiments on vertical plate radiators, supported by the Hyosung Corporation. These experiments were conducted in a group of 4 radiators, each with 40 plates of 3300mm. Three experiments were conducted, one in ONAN and the other two in the ODAN state. The experimental data reported are shown in Table 28.

Table 28 – Experimental data from [5]

	Experiment 1	Experiment 2	Experiment 3
Cooling State	ONAN	ODAN	ODAN
Oil Flow Rate per Radiator	0.001 m^3/s	0.0033 m^3/s	0.0042 m^3/s
Inlet Oil Temperature	89.3 ºC	88.8 ºC	88.3 ºC
Room Temperature	34.3 ºC	33.8 ºC	33.3 ºC

The four calculation methods seen in the previous subsections were applied in the conditions of Table 28 and the cooling capacity results were compared with the ones from the experiments. This comparison is presented in Figure 61 and Table 29.

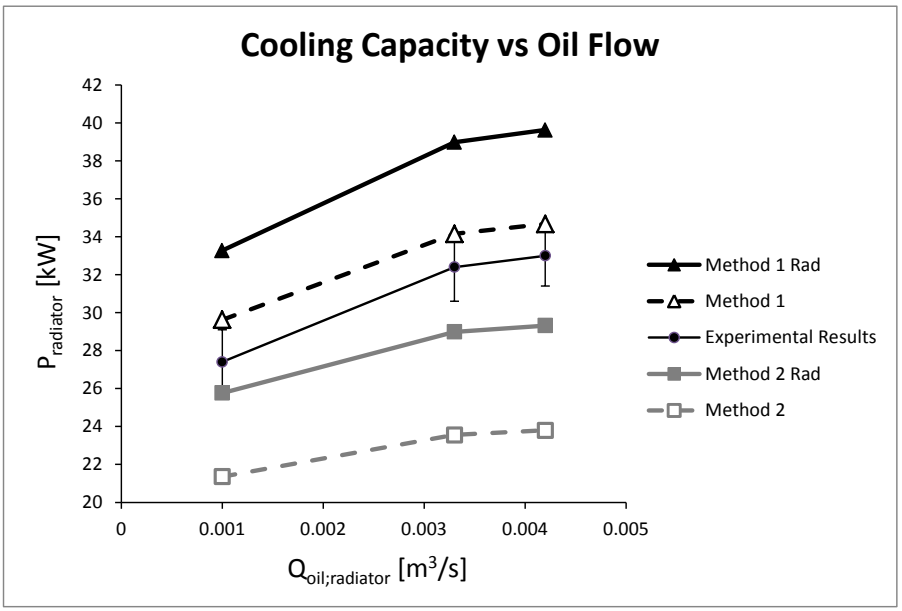

Figure 61 – Cooling capacity for different oil flow rates; comparison between the calculation procedures and the experiments from [5].

Table 29 – Experimental cooling capacities from [5] and calculation results.

	Cooling Capacity [kW]			Average Deviation from Experiments
	Experiment 1	Experiment 2	Experiment 3	
Experimental data from [5]	27.4±1.7	32.4±1.8	33.0±1.6	-
Method 1 Rad	33.3	39.0	39.6	21%
Method 1	29.6	34.2	34.7	6%
Method 2 Rad	25.8	29.0	29.3	9%
Method 2	21.4	23.6	23.8	26%

The results show that for this case study the predictions on cooling capacities from Method 1are above the experimental results and the ones from Method 2 are below the experiments. Looking only at this case, the results would suggest that the air flows in these experiments are between the isolated vertical plates situation and the fully developed state, since Method 1 uses a correlation for the first situation and Method 2 uses a correlation for the second. In fact this cannot be concluded, considering the other two case studies (subsections 4.2.1. and 4.2.2.) in which all calculation methods are below the experimental data. All the studied correlations for air natural convection that were analysed are not accurate for predicting the radiators' cooling capacity, especially for cases with small plates.

It is important to notice that between the three case studies the length of the plates is not the only parameter that is changed. The number of plates per radiator increases (7, 18 and 40 plates per radiator) as well as the oil flow rates per plate. These two parameters can also influence the different deviation from the calculations methodology.

5. Conclusions and Future Work

The modelling of vertical plate radiators for predicting their cooling performance was conducted successfully. Two calculation methodologies were developed, one for air forced convection and other for air natural convection. The first methodology applies to ONAF and ODAF cooling states and the second applies to ONAN and ODAN states. Both procedures turn out to be good techniques to design and optimize transformers' radiators, since the heat transfer correlations respond to the operational parameters variation (temperature, oil flow rate, air flow rate, etc.). For air forced convection cases, new correlations were developed using CFD simulation to improve the calculation methodology and it presented great accuracy when applied to the radiators of a real transformer (cooling capacity deviations from company tests of 3.9%). However, for the cases with air natural convection, the literature correlations provide results with high deviations comparatively to experiments and company tests.

The CFD models developed, consisting on rectangular prisms to represent individual air gaps between radiator's plates, proved to be a good and simple approach to evaluate air forced convection in radiators. Results show that the air flows between radiators' plates are not fully developed, causing a great impact in the heat transfer and errors in the cooling capacity estimated with literature correlations. The literature correlations applied in the smallest radiator plates present the highest deviations from CFD simulations, since in this case the air flow has a greater portion in the entry region. The created correlations adjust successfully to the simulations results and reflect the heat transfer enhancement by the entry region effect.

The average temperature of the walls and the air temperature are two parameters that should be analysed together. When these temperature values are changed, the cooling capacity does not change much if the difference between them is maintained. Cases with very low inlet velocities reveal high deviations between simulations and the calculation methodology, revealing that the turbulence model in simulation and/or the literature correlation aren't able to describe the heat transfer in the laminar region. This does not affect the analysis of air forced convection in radiators, since the air flow induced by the fans is always in the turbulent region.

A comparison between ventilating radiators with fans at the side and at the bottom was performed. On one hand, the results show that for the same air inlet velocities the side ventilation presents greater cooling capacities than bottom ventilation. On the other hand, introducing the same air flow rate the results are inverted. This happens because of the different cross sections on the side and on the bottom configurations, causing superior flow rates for side ventilation when fixing the velocities and superior velocities for bottom ventilation when fixing the air flow rates.

Cooling multiple radiators in series with side ventilation was compared with cooling the same amount of radiators with fans on the bottom. The results show that until a certain number of radiators the bottom ventilation is the most effective option, but for more radiators the side ventilations takes the lead. That number of radiators, in which the transition occurs, depends on the length of the plates and the number of fans that can be coupled in each configuration.

Regarding the air natural convection, four different calculation methodologies were evaluated in three case studies. Comparing to the other methodologies, Method 1 and Method Rad 1 presented cooling capacity results closer to the experimental data. However, since these methods use a correlation for isolated vertical plates and the results are above the experiments in the last case study, it can be concluded that the radiator plates don't behave like isolated surfaces in all situations. Method 2 Rad and Method 2 present high deviations for radiators with 800mm to 2200mm length (up to 55%) and lower ones for 3300mm (9% for Method 2 Rad and 26% for Method 2). Thus the correlation used in these methods is not accurate on predicting the cooling performance of vertical plate radiators. New correlations have to be developed, performing experiments or simulations, in order to enhance the accuracy of the calculation methodology for ONAN and ODAN cooling states.

Radiation reveals to be a mechanism of great importance in radiators heat dissipation, especially when air convection is natural (results reveal an increase on cooling capacity up to 29% by the addition of the radiation mode). Therefore radiation should be considered in the calculation methodologies.

Regarding future work, several studies can be conducted to better understand the radiators behaviour, namely:

- Evaluation of the air flow induced by fans. Although the created correlations for air forced convection provided accurate results, they depend on the air velocity and this parameter is estimated using the fans nominal air flow and the cross section between plates. This procedure may not be the most adequate since it doesn't reflect the distribution of the fans on the available area at the radiator.
- Study of the impact of the number of plates in the cooling performance. The number of plates in a radiator influences the amount of oil flow passing through each plate and consequently affects the cooling capacity. The impact of the number of plates has to be accounted to improve the prediction of the cooling performance.
- Evaluation of the correlations developed for air forced convection. Although the new correlations presented great accuracy for the studied transformer, they should be evaluated in other experimental case studies to validate their accuracy in different conditions.

6. References

[1] Efacec website. Page consulted on April 2014, http://www.efacec.pt

[2] R. M. Del Vecchio et al., *Transformer Design Principles: With Applications to Core-Form Power Transformers*, 2001.

[3] R. Hosseini et al., *Determination of OD cooling system parameters based on thermal modeling of power transformer winding*, Simulation Modelling Practice and Theory, 2008.

[4] European Commission website. Page consulted on May 2014, http://ec.europa.eu.

[5] M.-g. Kim et al., *Prediction and evaluation of the cooling performance of radiators used in oil-filled power transformer applications with non-direct and direct-oil-forced flow*, Exp. Therm. Fluid Sci., 2012.

[6] International Electrotechnical Commission, 2011. *IEC 60076-2 Power Transformers – Part 2: Temperature rise for liquid-immersed transformers*.

[7] Imad-U-Khan et al., *Dissolved Gas Analysis of Alternative Fluids for Power Transformers*, 2007.

[8] F. Delgado et al., *Fluid-thermal analysis of the cooling capacity of a commercial natural ester in a power transformer,* 2013.

[9] Engineering Craft Industries website. Page consulted on April 2014, http://www.engineeringcraft.in

[10] Eurocooler Document, *Technical Catalogue*, May 2009.

[11] Eurocooler Document, *Radiateurs pour Transformateurs, Documentation générale*, October 1996.

[12] Efaflu Document, *Cooling Fans and Pumps for Power Transformers*, May 2009.

[13] Krenz & Company, Inc. website. Page consulted on April 2014, http://www.krenzvent.com

[14] H. Nabati, J. Mahmoudi, *Numerical Modeling of a Plane Radiator Used in a Power Transformer Cooling System,* 2008.

[15] H. Nabati, J. Mahmoudi, *Simulation of Power Transformer' Cooling System in ONAN State*, 2008.

[16] R. Fdhila et al., *Thermal modeling of power transformer radiators using a porous*

medium based CFD approach, 2011.

[17] F. P. Incropera et al., *Fundamentals of Heat and Mass Transfer*, 7th Edition, 2011.

[18] S.W. Churchill and H.S. Chu, *Correlating Equations for Laminar and Turbulent Free Convection from a Vertical Plate*, 1975.

[19] W. Elenbaas, *Heat Dissipation of Parallel Plates by Free Convection*, 1942.

[20] W. M. Rohsenow et al., *Handbook of Heat Transfer*, 3rd Edition, 1998.

[21] Hugh W. Coleman and W. Glenn Steele, *Experimentation, Validation, and Uncertainty Analysis for Engineers*, 3rd Edition, 2009.

Annex A: Oil and Air Properties

The reference of the mineral oil used in Efacec's transformers is Nynas Taurus. This oil has a volumetric thermal expansion coefficient of 0.00064 K^{-1}. The equations for the other properties depending on temperature were taken from company graphs and are showed from equation A.1 to A.4. In these equations the temperature is in ºC.

$$c_{p_{oil}} = 3.4566 \cdot T + 1796.5 \quad \text{(A.1)}$$

$$k_{oil} = -0.000077 \cdot T + 0.132949 \quad \text{(A.2)}$$

$$\rho_{oil} = 868 \cdot [1 - 0.00064 \cdot (T - 20)] \quad \text{(A.3)}$$

$$\mu_{oil} = 1.433 \cdot 10^{-7} \cdot \exp\left(\frac{3479.5}{T + 273.15}\right) \quad \text{(A.4)}$$

The air properties were taken using tabulated data from [17] that was plotted. The equations were extracted with trend lines. The plots are in Figures A.1 to A.4 and the equations are presented in A.5 to A.8. The volumetric thermal expansion coefficient was calculated with A.9 considering the air an ideal gas. In these equations the temperature is in kelvin.

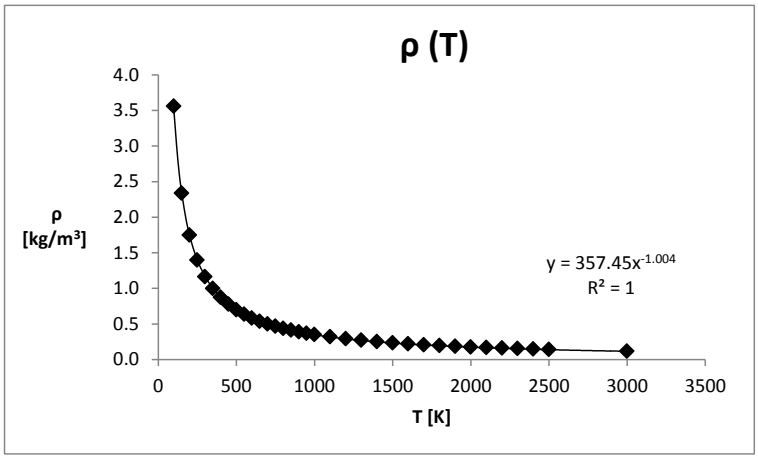

Figure A.1 – Air density as a function of temperature.

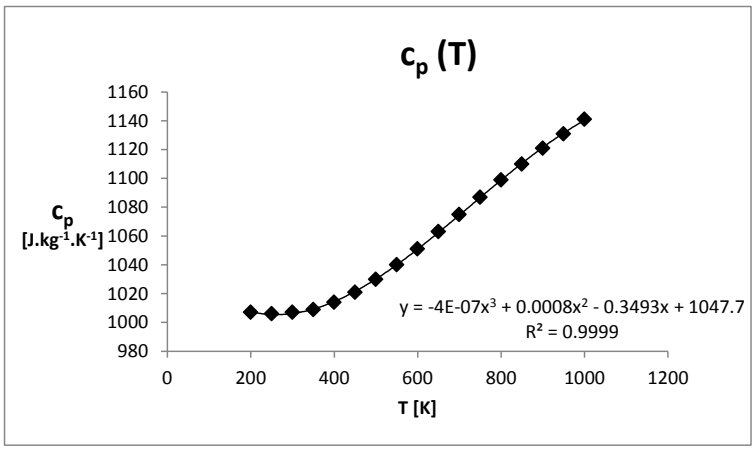

Figure A.2 – Air specific heat at constant pressure as a function of temperature.

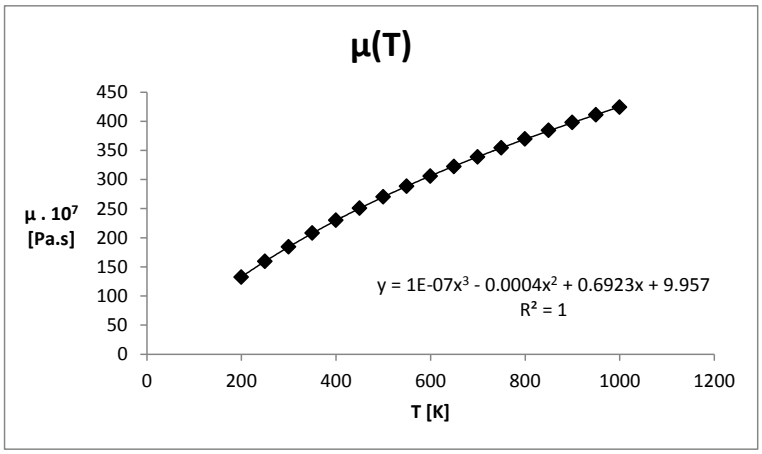

Figure A.3 – Air dynamic viscosity as a function of temperature.

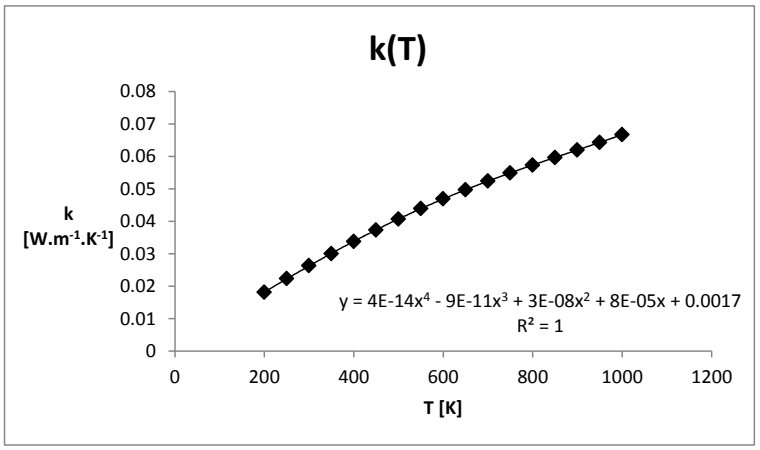

Figure A.4 – Air density as a function of temperature.

$$\rho_{air} = 357.45 \cdot T^{-1.004} \quad \text{(A.5)}$$

$$c_{p_{air}} = -4 \cdot 10^{-7} \cdot T^3 + 8 \cdot 10^{-4} \cdot T^2 - 0.3493 \cdot T + 1047.7 \quad \text{(A.6)}$$

$$\mu_{air} = (1 \cdot 10^{-7} \cdot T^3 - 4 \cdot 10^{-4} \cdot T^2 + 0.6923 \cdot T + 9.957) \cdot 10^{-7} \quad \text{(A.7)}$$

$$k_{air} = 4 \cdot 10^{-14} \cdot T^4 - 9 \cdot 10^{-11} \cdot T^3 + 3 \cdot 10^{-8} \cdot x^2 + 8 \cdot 10^{-5} \cdot T + 0.0017 \quad \text{(A.8)}$$

$$\beta = 1/T \quad \text{(A.9)}$$

Annex B: Parameters of CFD Simulations

The values used in CFD simulation for all parameters are listed in Table B.1.

Table B.1 – Values for the CFD simulation parameters

	$T_{wall;top}$ [ºC]	ΔT_{wall} [ºC]	L [mm]	$T_{air;in}$ [ºC]	$v_{air;in}$ [m/s]	Plates in Series
	y_1	y_2	y_3	y_4	y_5	y_6
Base Case (x_0)	50.9	14.1	2200	25.8	4.10	1
x_1	43.9	0	800	0	0.35	2
x_2	63.8	7.1	1000	40	0.56	4
x_3	75.8	21.2	1500		0.85	6
x_4			3300		0.97	
x_5					1.06	
x_6					1.50	
x_7					1.55	
x_8					2.33	
x_9					2.39	
x_{10}					2.67	
x_{11}					2.91	
x_{12}					3.59	
x_{13}					4.48	

A total of 56 simulations were performed by making different combinations of the parameters' values. The first and second simulations were conducted for the base case values and for bottom and side ventilations. The other 54 combinations are listed in Table B.2 and Table B.3, for bottom and side ventilations respectively. The combinations are identified mentioning the variables that are different from the base case, using the code presented in Table B.1.

Table B.2 – Combinations for bottom ventilation

$y_1 - x_2$	$y_1 - x_3$	$y_1 - x_3; y_3 - x_1$	$y_1 - x_2; y_3 - x_4$	$y_1 - x_1; y_2 - x_1$
$y_3 - x_2$	$y_3 - x_3$	$y_3 - x_4$	$y_4 - x_1$	$y_3 - x_1; y_5 - x_{12}$
$y_5 - x_6$	$y_5 - x_9$	$y_5 - x_{12}$	$y_5 - x_{13}$	$y_3 - x_1; y_5 - x_{13}$
$y_3 - x_1$	$y_2 - x_3; y_3 - x_4$	$y_3 - x_1; y_5 - x_6$	$y_3 - x_1; y_5 - x_9$	$y_3 - x_1; y_4 - x_1$
$y_2 - x_2$	$y_1 - x_2; y_4 - x_2$			

Table B.3 – Combinations for side ventilation

$y_5 - x_1$	$y_5 - x_{11}$	$y_3 - x_1; y_5 - x_1$	$y_3 - x_1; y_5 - x_{11}$	$y_6 - x_2; y_5 - x_1$
$y_5 - x_2$	$y_5 - x_{12}$	$y_3 - x_1; y_5 - x_4$	$y_3 - x_1; y_5 - x_{12}$	$y_6 - x_2; y_5 - x_7$
$y_5 - x_3$	$y_5 - x_{13}$	$y_3 - x_1; y_5 - x_6$	$y_3 - x_1; y_5 - x_{13}$	$y_6 - x_2; y_5 - x_{10}$
$y_5 - x_4$	$y_3 - x_1$	$y_3 - x_1; y_5 - x_7$	$y_6 - x_1; y_5 - x_1$	$y_6 - x_2; y_5 - x_{13}$
$y_5 - x_5$	$y_6 - x_1$	$y_3 - x_1; y_5 - x_8$	$y_6 - x_1; y_5 - x_7$	
$y_5 - x_6$	$y_6 - x_2$	$y_3 - x_1; y_5 - x_9$	$y_6 - x_1; y_5 - x_{10}$	
$y_5 - x_9$	$y_6 - x_3$	$y_3 - x_1; y_5 - x_{10}$	$y_6 - x_1; y_5 - x_{13}$	

Annex C: Experiments Uncertainty Analysis

According to [21], the random uncertainty with 95% confidence for sample populations can be calculated with equation C.1.

$$P_X = t_{95} \cdot S_X \quad \text{(C.1)}$$

Where P_X, t_{95} and S_x are the random uncertainty, the t-distribution for a 95% confidence interval and the sample standard deviation, respectively. For the performed experiments three variables were measured: the oil inlet temperature, outlet temperature and volumetric flow rate. Considering the number of measures (*N*) for each variable and the degrees of freedom (*N*-1), the random uncertainties were estimated and are presented in tables C.1 and C.2 for the experiments 1 and 2, respectively.

Table C.1 – Random uncertainty estimation for experiment 1

	$T_{oil;in}$ [ºC]	$T_{oil;out}$ [ºC]	Q_{oil} [m^3/h]
Average	36.41	32.09	0.48
N	227	227	18
Deg. of Freedom	226	226	17
S_X	0.1190	0.1133	0.009884
t_{95}	1.971	1.971	2.110
P_X	0.23	0.22	0.02

Table C.2 – Random uncertainty estimation for experiment 2

	$T_{oil;in}$ [ºC]	$T_{oil;out}$ [ºC]	Q_{oil} [m^3/h]
Average	57.48	47.73	0.4688
N	74	74	11
Deg. of Freedom	73	73	10
S_X	0.1221	0.1240	0.01233
t_{95}	1.993	1.993	2.228
P_X	0.24	0.25	0.03

The systematic uncertainty (B_X) was assumed equal to the measurement accuracy of the temperature sensors and the flow meter, taken from these apparatus catalogues. The total uncertainties (U_X) of the variables were calculated using equation C.2 and are presented in tables C.3 and C.4 for the experiments 1 and 2, respectively.

$$U_x = \sqrt{P_x^2 + B_x^2} \quad \text{(C.2)}$$

Table C.3 – Uncertainties for experiment 1

	$T_{oil;in}$ [ºC]	$T_{oil;out}$ [ºC]	Q_{oil} [m^3/h]
P_X	0.23	0.22	0.02
B_X	0.50	0.50	0.024
U_X	0.55	0.55	0.031

Table C.4 – Uncertainties for experiment 2

	$T_{oil;in}$ [ºC]	$T_{oil;out}$ [ºC]	Q_{oil} [m^3/h]
P_X	0.24	0.25	0.03
B_X	0.50	0.50	0.024
U_X	0.55	0.56	0.038

The cooling capacity was calculated using the average values of the temperatures and the oil flow rate. Using the software EES (*Engineering Equation Solver*), the uncertainty propagation was made and consequently the total uncertainty for the cooling capacity was obtained with a confidence interval of 95%. The final results are shown in figures C.1 and C.2 for the experiments 1 and 2, respectively.

Unit Settings: SI C kPa J mass deg

Variable±Uncertainty	Partial derivative	% of uncertainty
P = 954.8±182.6 [W]		
Q_{oil} = 0.4835±0.031 [m^3/h]	$\partial P / \partial Q_{oil}$ = 1975	11.24 %
$T_{oil,in}$ = 36.41±0.55	$\partial P / \partial T_{oil,in}$ = 221.7	44.60 %
$T_{oil,out}$ = 32.09±0.55	$\partial P / \partial T_{oil,out}$ = -220.6	44.16 %

Figure C.1 – Final results for experiment 1.

Unit Settings: SI C kPa J mass deg

Variable±Uncertainty	Partial derivative	% of uncertainty
P = 2135±243.9 [W]		
Q_{oil} = 0.4688±0.038 [m^3/h]	$\partial P / \partial Q_{oil}$ = 4554	50.35 %
$T_{oil,in}$ = 57.48±0.55	$\partial P / \partial T_{oil,in}$ = 220.1	24.64 %
$T_{oil,out}$ = 47.73±0.56	$\partial P / \partial T_{oil,out}$ = -217.8	25.01 %

Table C.2 – Final results for experiment 2.